Ann. Rev. Astron. Astrophys. 1985. 23 : 169–224

RADIO EMISSION FROM THE SUN AND STARS

George A. Dulk

Department of Astrophysical, Planetary and Atmospheric Sciences,
University of Colorado, Boulder, Colorado 80309

1. INTRODUCTION

Radio astronomy of the stars is now a burgeoning new field of study; at the same time, radio astronomy of the Sun has reached a high level of maturity and sophistication. Most of the radio emission processes occurring on stars have probably been identified from solar studies, but only a fraction of the contexts of the emission have been encountered. It is timely to review the progress in stellar observations, to outline the circumstances in which various radiation mechanisms occur on the Sun, and to assemble some useful formulae for semiquantitative analysis of radio observations.

In this review we concentrate on the radiation that is emitted by "normal" stars, defined here to include those appearing on classical Hertzsprung-Russell diagrams. Specifically, we include the range from supergiants to white dwarfs but exclude pre-main-sequence stars and condensed objects such as neutron stars; the last two classes can have different radio emission processes. In Section 2 we discuss the mechanisms for both steady, quiescent emission (usually due to incoherent radiation processes) and intense, strongly varying outbursts (often due to coherent processes). Included are discussions of bremsstrahlung, gyrosynchrotron emission (including gyroresonance emission at the nonrelativistic limit, and synchrotron emission at the relativistic limit), electron-cyclotron masers, and plasma radiation. In Section 3 we discuss how these mechanisms are manifested in various kinds of solar radiation, in Section 4 we examine the stellar manifestations, and in Section 5 we give our conclusions.

0066–4146/85/0915–0169$02.00

2. EMISSION MECHANISMS

General Remarks

The radio emission processes described here range from very simple to quite complex. As we deal almost entirely with continuum radiation, we do not encounter the special problems associated with radiative transfer in spectral lines. Much radio radiation is due to individual electrons when they are accelerated either because of collisions with ions (bremsstrahlung) or because of spiraling in a magnetic field (gyrosynchrotron emission); the result is "incoherent" radiation. In some circumstances there can be very efficient conversion of electron energy into some natural wave mode of the plasma, such as electron-cyclotron waves (transverse, electromagnetic waves) or Langmuir waves (longitudinal, electrostatic waves). These waves are in the radio-frequency domain because the characteristic frequencies of the relevant plasmas are typically $\lesssim 10^{10}$ Hz; the main characteristic frequencies are the electron plasma frequency

$$\nu_p = \omega_p/2\pi = [n_e e^2/\pi m_e]^{1/2} \approx 9000\, n_e^{1/2}, \qquad 1.$$

and the electron-cyclotron frequency

$$\nu_B = \Omega_e/2\pi = eB/2\pi m_e c \approx 2.8 \times 10^6 B. \qquad 2.$$

Resonances between particles and characteristic waves can occur, and these can rapidly extract any free energy that might exist in the electron distribution; anisotropies of various kinds are probably the most important form of free energy. Plasmas with free energy, i.e. in nonequilibrium, can only exist when the electron-electron and electron-ion collision frequencies

$$\nu_{ee} \approx 13.7\, n_e T^{-3/2}\,(14.7 - \tfrac{1}{2}\ln n_e + \ln T) \qquad (T > 7.2 \times 10^4\ \mathrm{K}) \qquad 3.$$

$$\nu_{ei} \approx 13.7\, n_e T^{-3/2} \times \begin{cases} (9.1 - \tfrac{1}{2}\ln n_e + \tfrac{3}{2}\ln T - \ln Z_i) & (T < 1.4 \times 10^5\ \mathrm{K}) \\ (15.1 - \tfrac{1}{2}\ln n_e + \ln T - \ln Z_i) & (T > 1.4 \times 10^5\ \mathrm{K}) \end{cases} \qquad 4.$$

are neither as high as the resonance frequencies nor so high as to restore the plasma quickly to equilibrium and thus quench the instabilities; this is the major reason that amplified radiation is generally confined to radio frequencies. The instabilities can be of two kinds: reactive instabilities in which bunching of particles at particular wave phases is important, and resistive instabilities of random phase where the resistance acts in negative fashion; the latter are probably the more important kind in circumstances of present interest. In resistive instabilities, amplification (negative absorption) carries the intensity of the particular wave modes to very high levels

and leads to "coherent emission." If the resulting waves are electromagnetic, they might escape directly, as is perhaps the case in the electron-cyclotron maser; if the waves are trapped or nontraveling, subsequent conversion to transverse waves must occur first, as in plasma radiation.

The sources of radio radiation are often optically thick (in contrast to X-radiation), and care must be taken not to apply optically thin formulae in these cases; errors of many orders of magnitude have appeared in the literature because of improper application. If we consider only incoherent radiation for the moment, the specific intensity of radiation from optically thick sources only depends on, and only contains information about, the average energy of the emitting electrons (their temperature in the case of thermal electrons). In contrast, the specific intensity of radiation from optically thin sources depends on the density and energy distribution of emitting electrons, the magnetic field, and the distributions of each along the line of sight. Thus for optically thin sources, the magnetic field strength and direction are potentially derivable from radio observations of intensity and polarization, but either additional assumptions or data (e.g. from X-ray observations or radio brightness spectra) are usually necessary to separate the properties of the magnetic field from those of the electron distribution. If only the flux density is measured, rather than the specific intensity, it contains less information (the integration of intensity over the projected area of the source).

Brightness Temperature and Radiative Transfer

We now set out the definitions of brightness temperature, effective temperature, and the relations from radiative transfer in a form that is useful for the interpretation of radio observations. The equation of radiative transfer is usually written in terms of the specific intensity I_ν, but at radio frequencies where $h\nu \ll kT$, it is convenient to change variables from I_ν to brightness temperature T_b, where

$$I_\nu = kT_b\nu^2/c^2 \text{ erg cm}^{-2} \text{ s}^{-1} \text{ Hz}^{-1} \text{ sr}^{-1}. \quad 5.$$

It is also convenient to replace the source function S_ν by T_{eff}, the effective temperature of the radiating electrons, using the relation

$$S_\nu = \eta_\nu/\kappa_\nu = kT_{\text{eff}}\nu^2/c^2. \quad 6.$$

In the case of a Maxwellian electron distribution of temperature T, T_{eff} is equal to T irrespective of the emitting mechanism, frequency, or polarization mode; in addition, the emissivity η_ν is related to the absorption coefficient κ_ν by Kirchhoff's Law

$$\eta_\nu = \kappa_\nu kT\nu^2/c^2 \text{ erg cm}^{-3} \text{ s}^{-1} \text{ Hz}^{-1} \text{ sr}^{-1}. \quad 7.$$

In contrast, for a nonthermal electron distribution, $T_{\rm eff}$ generally is a function of both frequency and polarization mode (Wild et al. 1963). Note that the usual factor of 2 is missing from Equations 5 and 6 because we define I_ν and S_ν for each of the orthogonal polarizations separately and have

$$I_\nu^{\rm tot} = I_\nu^{\rm p1} + I_\nu^{\rm p2}. \qquad 8.$$

Equations 5 and 6 allow us to write the radiative transfer equation in the form

$$dT_{\rm b}/d\tau_\nu = -T_{\rm b} + T_{\rm eff}, \qquad 9.$$

or, as an integral, using the geometry of Figure 1,

$$T_{\rm b} = \int_0^{\tau_\nu} T_{\rm eff} \exp(-t_\nu)\, dt_\nu + T_{\rm bo} \exp(-\tau_\nu). \qquad 10.$$

Equations 9 and 10 and the gyrosynchrotron formulae given below are valid only for media in which the density is so low that the index of refraction is nearly unity. This situation, which applies in a wide range of astrophysical situations, is the only one for which the formulae of interest can be greatly simplified. When the index of refraction deviates significantly from unity, it must be included properly in Equations 9 and 10, and medium suppression (the Razin-Tsytovich effect) must also be taken into account. Specifically, medium suppression is important when $\nu < 20\ n_e/B$ (see Ginzburg & Syrovatskii 1969).

In the special case of an isolated source with constant $T_{\rm eff}$, Equation 10 reduces to

$$T_{\rm b} = T_{\rm eff}[1-\exp(-\tau_\nu)], \qquad 11.$$

$$T_{\rm b} = T_{\rm eff} \qquad (\text{if } \tau_\nu \gg 1) \qquad 12.$$

$$= T_{\rm eff}\tau_\nu = (c^2/k\nu^2)\eta_\nu L \qquad (\text{if } \tau_\nu \ll 1), \qquad 13.$$

where L is the dimension of the source along the line of sight.

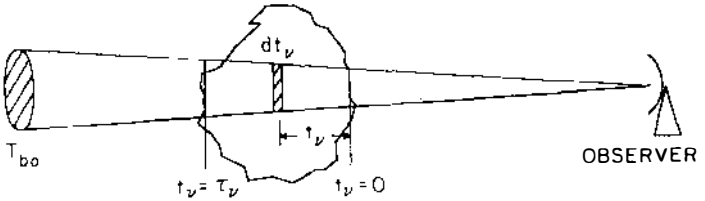

Figure 1 Geometry for Equation 10, illustrating a source of optical depth τ_ν located in front of a possible background of brightness temperature $T_{\rm bo}$.

For incoherent radiation, Equations 12 and 13 are of considerable importance and utility. They show that such radiation cannot attain a value of T_b higher than T_{eff}. Further, the source function T_{eff} is related to the average energy of the emitting particles by $\langle E \rangle = kT_{eff}$. For example, for monoenergetic electrons of $T_{eff} = E_o/k$ or a Maxwellian distribution of $T_{eff} = T = E_o/k$, we have $T_{b,max} = T_{eff}$, e.g. $T_{b,max} = 1.16 \times 10^7$ K if $E_o =$ 1 keV or 1.16×10^{10} K if $E_o = 1$ MeV. In the case of a power-law electron distribution, T_{eff} is determined by the average energy of the electrons contributing most strongly to the intensity at the particular frequency and polarization mode. If that average energy and hence brightness temperature is to be high, the circumstances must be such that the more numerous lower-energy electrons do not emit and absorb efficiently; in general, this requires a low magnetic field strength (see below). Under solar and stellar conditions, field strengths tend to be large and electron energies low (compared with, for example, those of extragalactic sources), so that T_{eff} and T_b of incoherent emission are usually limited to about 10^9 to 10^{10} K. Observed values substantially above these thus imply a coherent mechanism, such as maser or plasma radiation.

The flux density S (for one polarization) of a radio source is related to the brightness temperature by the relation

$$S = kv^2/c^2 \int T_b \, d\Omega, \qquad 14.$$

where $d\Omega$ is a differential solid angle and the integral is over the projected area of the source.

The general theory of polarization of the radiation is, in general, fairly complex because of coupling among the various Stokes parameters (e.g. Melrose 1980a, p. 196). However, under solar and stellar conditions the characteristic modes of the plasma (the o- and x-modes) are usually circular except when propagation is nearly perpendicular to the magnetic field (within $|\pi/2 - \theta| < \nu_B/2v$). The observed sense of polarization usually reflects the sense of the magnetic field in the source region. A change in the sense of circular polarization can occur because of weak mode coupling in a transverse region somewhere along the ray path, but for (the intensively studied) solar bursts, no unambiguous evidence for polarization reversals has been found.

The degree of circular polarization r_c is

$$r_c = (T_{b,x} - T_{b,o})/(T_{b,x} + T_{b,o}). \qquad 15.$$

When $\tau_\nu \ll 1$ for both modes, Equation 15 can be replaced by

$$r_c = (\eta_{\nu,x} - \eta_{\nu,o})/(\eta_{\nu,x} + \eta_{\nu,o}) \qquad (\tau_\nu \ll 1). \qquad 16.$$

[In some circumstances the polarization ellipse of a characteristic mode, the x-mode say, differs significantly from circular, i.e. the axial ratio T_x deviates significantly from unity; in these cases the right-hand side of Equation 16 needs to be multiplied by $2T_x/(T_x^2+1)$.] Because the emissivity of the x-mode is the higher, the polarization of free-free and gyrosynchrotron radiation is the sense of the x-mode and can be quite large, especially for gyrosynchrotron emission. On the other hand, when $\tau_\nu \gg 1$ for both modes, the polarization of free-free and gyrosynchrotron radiation goes to zero for a thermal plasma; for a nonthermal, say power-law, distribution, the polarization is low ($\lesssim 0.2$), and for a homogeneous slab source it is in the sense of the o-mode. The reason for o-mode polarization is that the ratio of emissivity to absorption coefficient is larger for the o-mode than for the x-mode, and electrons of slightly higher average energy produce o-mode emission in optically thick sources.

For plasma radiation the polarization is generally (but not always; see below) in the sense of the o-mode.

Considerable caution should be used in interpreting polarization measurements for the following reasons: First, for Equation 15 to be valid, there can be no significant variation in plasma properties along the line of sight within the emission region, i.e. no significant changes in B, θ, or $T_{\rm eff}$. Second, as defined, the polarization applies to brightness temperature, not to flux density. The latter involves an integration not only along the line of sight but also over all parts of the source; therefore, if B, θ, or $T_{\rm eff}$ vary with position in the source, as frequently is the case, then the polarization of flux density is the average (weighted by T_b) of the polarization of brightness temperature. In particular, for gyrosynchrotron emission, x-mode polarization from optically thin boundaries of sources can mask the o-mode polarization of optically thick central parts.

Another useful quantity for diagnostics is $\nu_{\rm peak}$, the frequency of peak flux density in a spectrum that changes from a positive to a negative slope, as depicted in Figure 2. The peak occurs at that frequency where $\tau_\nu = \kappa_\nu L \approx 1$. For free-free bremsstrahlung, $\nu_{\rm peak}$ depends on the emission measure

$$EM = \int n_e^2 \, ds. \qquad 17.$$

For gyrosynchrotron emission, $\nu_{\rm peak}$ depends very strongly on the magnetic field strength and the average electron energy, but very weakly on electron numbers or path lengths. Thus if the electron energy can be estimated (e.g. from hard X-ray data), the field strength can be found.

Bremsstrahlung

When individual electrons are deflected in the coulomb fields of ions owing to their accelerated motion, they produce bremsstrahlung, or free-free

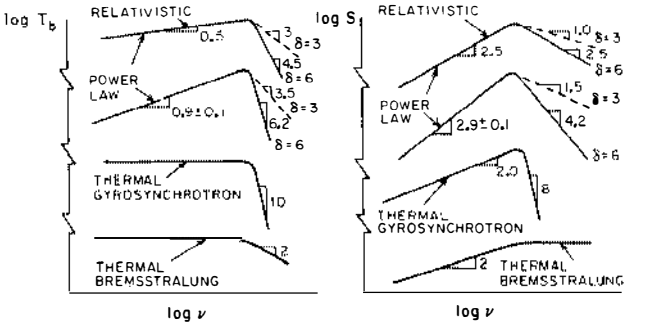

Figure 2 Schematic spectra of brightness temperature and flux density. The upper three curves are for gyrosynchrotron radiation, the top one for a power-law distribution of highly relativistic electrons with electron spectral indices $\delta = 3$ and 6, and the next one for mildly relativistic electrons.

emission. The inverse process, free-free absorption, occurs when electrons begin to oscillate in resonance with the electric field of a wave and then electron-ion collisions destroy the oscillation; this decreases the wave energy and heats the plasma. In the remainder of this section, we follow the treatment of bremsstrahlung given by Scheuer (1960) and Melrose (1980a, pp. 78, 182).

For radio waves, distant encounters of electrons with ions (causing small-angle deflections) are much more important than the relatively rare close encounters and large deflections. The average emissivity of electrons in a plasma is calculated by starting with the energy radiated by an electron of velocity v passing at a distance d from an ion of charge Z_i, and then multiplying by the rate of such encounters and integrating over d and v. Here we consider only Maxwellian velocity distributions, for which $v = (kT/m)^{1/2}$.

$G(T, \omega)$, that is proportional to the logarithm of d_{max}/d_{min}, where d_{max} and d_{min} are the maximum and minimum impact parameters. Because collisions at given d lead to emission only at $\omega \lesssim v/d$, we have $d_{max} \approx v/\omega$. The minimum impact parameter d_{min} differs according to the average energy of the electrons. For low-energy electrons, d_{min} is approximately the distance for which the electron suffers a 90° deflection, and then

$$G(T, v) = \frac{\sqrt{3}}{\pi} \ln\left(\frac{2(kT)^{3/2}}{\Gamma \omega Z_i m^{1/2} e^2}\right), \qquad 18.$$

where $\Gamma \approx 1.781$ is Euler's constant. For higher-energy electrons, d_{min} is related to the de Broglie wavelength, and the Gaunt factor is

$$G(T, v) = \frac{\sqrt{3}}{\pi} \ln\left(\frac{2kT}{hv}\right). \qquad 19.$$

At high frequencies where $h\nu \gtrsim kT$ (e.g. in the X-ray range), the above forms for the Gaunt factor do not apply and must be replaced by appropriate quantum calculations.

The absorption coefficient for thermal electrons, including the above factors, is

$$\kappa_\nu \approx \sum_i \frac{1}{3c}\left(\frac{2}{\pi}\right)^{1/2} \frac{\nu_p^2}{\nu^2} \frac{4\pi Z_i^2 n_i e^4}{m^{1/2}(kT)^{3/2}} \cdot \frac{\pi}{\sqrt{3}} G(T,\nu) \qquad 20.$$

$$\approx 9.78 \times 10^{-3} \frac{n_e}{\nu^2 T^{3/2}} \sum_i Z_i^2 n_i$$

$$\times \begin{cases} 18.2 + \ln T^{3/2} - \ln \nu & (T < 2 \times 10^5 \text{ K}) \\ 24.5 + \ln T - \ln \nu & (T > 2 \times 10^5 \text{ K}). \end{cases}$$

The emissivity η_ν is related to κ_ν by Kirchhoff's Law (Equation 7).

For many purposes a simpler form of Equation 20 is useful. Assuming a fully ionized hydrogen-helium plasma and taking typical values of $\nu \sim 10^8$ Hz and $T \sim 10^6$ K for the logarithmic term, we have

$$\kappa_\nu \approx 0.2\, n_e^2 T^{-3/2}\, \nu^{-2} \text{ cm}^{-1}. \qquad 21.$$

In the presence of a magnetic field, the x-mode is emitted and absorbed more strongly than the o-mode. For a homogeneous, thermal, optically thin plasma, in cases where the quasi-circular approximations apply, this leads to a net polarization in the sense of the x-mode:

$$r_c \approx 2 \cos\theta(\nu_B/\nu). \qquad 22.$$

If the plasma is isothermal and optically thick, the polarization is zero.

Gyroresonance and Gyrosynchrotron Emission

When a plasma contains a magnetic field, accelerations due to particle collisions can often be negligible in comparison with those due to gyration around the field lines. In place of free-free emission and absorption, we then have gyroresonance (or cyclotron) emission and absorption in the case of nonrelativistic particles (Lorentz factor $\gamma = 1$), gyrosynchrotron in the case of mildly relativistic particles (γ less than about 2 or 3), and synchrotron in the case of highly relativistic particles ($\gamma \gg 1$). Because free-free emission goes as $n^2 T^{-1/2}$ and gyrosynchrotron emission goes as $nT^\alpha B^\beta$ (with α, $\beta > 1$), it follows that the former dominates if the density is high enough or if the temperature or field strength is low enough. In some circumstances the different frequency dependences of the two kinds of emission lead to one dominating at low frequencies and the other at high.

In the case of gyroresonance emission and absorption, thermal electron distributions are of most interest because the average energy of the electrons is low, leading to frequent collisions and generally to Maxwellian distributions. Emission is concentrated at the fundamental frequency $\omega = \Omega_e$ and at harmonics $s \lesssim 10$. Radiation at the fundamental frequency ($s = 1$) is directed mainly along the magnetic field [$P(\theta) \propto \cos^2 \theta$], and radiation at low harmonics is mainly at moderate angles [$P(\theta) \propto \cos^2 \theta \sin^{2s} \theta$]. In the opposite limit of synchrotron radiation, electron collisions are rare, a non-Maxwellian tail is generally dominant, and the distribution is usually well described by a power law. Emission is distributed over a broad continuum at high harmonics near $s \approx (\gamma \sin \theta)^3$, i.e. near frequency $\omega \approx \Omega_e \gamma^2 \sin \theta$. Emission is directed very strongly in the direction of the instantaneous electron motion, which leads, for approximately isotropic distributions, to a peak of radiation perpendicular to the field. In the intermediate case of gyrosynchrotron radiation, both thermal and power-law distributions are of interest, emission at harmonics $10 \lesssim s \lesssim 100$ is of major importance, and the emission from approximately isotropic electrons has a broad maximum perpendicular to the field.

In the following we give the main emission and absorption properties for each of these cases, following the approach of Melrose (1980c, 1985b).

Gyroresonance Radiation From Thermal Electrons

In the nonrelativistic limit, the emission from a single electron is at the sth harmonic of the Doppler-shifted gyrofrequency, and (for a distribution of electrons) those that dominate in emission and absorption processes satisfy the resonance condition

$$\omega = s\Omega_e/\gamma + k_\parallel v_\parallel \approx \frac{s\Omega_e}{\gamma}(1 + \mu\beta \cos \alpha \cos \theta), \qquad 23.$$

where $\mathbf{k}$ is the wave vector, μ is the index of refraction, $\beta = v/c$, and α is the electron pitch angle. In the nonrelativistic limit, it is adequate to put $\gamma = 1$ and to retain only the leading terms of the power series describing the Bessel functions that appear in the expression for the emissivity. Then, integrating over the electron velocities of a Maxwellian distribution, one obtains the following results:

Range of validity: $$s^2\beta_0^2 \ll 1 \quad \text{where} \quad \beta_0^2 = kT/mc^2. \qquad 24.$$

Kirchhoff's Law: $$\eta_\nu(s, \theta) = \mu_\sigma^2 \frac{\nu^2}{c^2} \frac{\partial}{\partial \omega}(\omega\mu_\sigma) kT\kappa_\nu(s, \theta). \qquad 25.$$

For $|\pi/2 - \theta| \gtrsim \nu_B/2\nu$ and $\nu_B/2\nu \ll 1$, we have

$$\kappa_\nu(s,\theta) = \frac{\pi^2}{4c} \frac{1}{\mu_\sigma \frac{\partial}{\partial\omega}(\omega\mu_\sigma)} \frac{\nu_p^2}{\nu} \frac{s^2}{s!} \times \left(\frac{s^2\beta_o^2 \sin^2\theta}{2}\right)^{s-1} \frac{1}{\beta_o|\cos\theta|} \times \exp\left[-\frac{(1 - s\nu_B/\nu)^2}{2\mu_o^2\beta_o^2\cos^2\theta}\right](1-\sigma|\cos\theta|)^2, \quad 26.$$

where $\sigma = +1$ for the o-mode, $\sigma = -1$ for the x-mode, and μ_σ is the index of refraction (hereafter equal to unity). Because of the exponential factor, κ_ν decreases rapidly at frequencies differing from $\nu = s\nu_B$, and it is convenient to define an alternate absorption coefficient, averaged over the profile of an individual harmonic:

$$\langle\kappa_\nu(s,\theta)\rangle = \int_{-\infty}^{\infty} \kappa_\nu(s,\theta)\frac{d\nu}{\nu_B} = \left(\frac{\pi}{2}\right)^{5/2} \frac{2}{c} \frac{\nu_p^2}{\nu} \frac{s^2}{s!} \left(\frac{s^2\beta_o^2 \sin^2\theta}{2}\right)^{s-1} \times (1-\sigma|\cos\theta|)^2, \quad 27.$$

where the effective path length L to be used with Equation 27 is the scale length of the magnetic field $L_B = B/\nabla B$. (A smaller length is appropriate to Equation 26: $L = 2L_B\beta_o \cos\theta$.)

At angles $\theta \gtrsim 60°$ the quasi-circular approximations break down, and while Equations 26 and 27 continue to be approximately valid for the x-mode, they are not valid for the o-mode. At $\theta = \pi/2$, we have

$$\kappa_\nu(s,\pi/2)|_{\text{o-mode}} = \beta_o^2\kappa_\nu(s,\pi/2)|_{\text{x-mode}}. \quad 28.$$

Gyrosynchrotron Radiation From Thermal Electrons

For temperatures in the range $\approx 5 \times 10^7$ to $\approx 5 \times 10^9$ K, emission and absorption are usually important in the range of harmonics ≈ 10 to ≈ 100. One cannot then use only the leading terms of a power-series expansion of the Bessel functions (as for nonrelativistic electrons) or the Airy integral approximation (as for relativistic electrons). Numerical calculations are often used, but they are time consuming and inconvenient. Petrosian (1981) has derived simplified analytical expressions for the radiation that are quite accurate over a fairly wide range of s and θ, and Robinson & Melrose (1984) have corrected and extended these expressions to the point that they are valid for all $s > 5$. We give the Robinson & Melrose results below

(Equation 29a). Also, in Equation 29b we give a considerably simpler expression from Dulk et al. (1979), one whose range of validity is restricted to $10^8 \lesssim T \lesssim 10^9$ K and $10 \lesssim s \lesssim 100$. We also give expressions for the emissivity in terms of the absorption coefficient, the degree of circular polarization in the case of small optical depth, and the frequency of maximum flux density ν_{peak} for a homogeneous source. (For thermal electrons, ν_{peak} is the frequency at which $\tau \approx 2.5$.) Because ν_{peak} depends sensitively on the magnetic field strength and temperature but not on the density or path length, it is a good diagnostic for B if the temperature is known (e.g. from X-ray data).

$$\frac{\kappa_\nu B}{N} \approx 2.67 \times 10^{-9} \frac{\mu^2(1-15/8\mu)}{n_\sigma^2 \sin^3\theta} \frac{\gamma_o^{3/2}(\gamma_o}{1+T_\sigma^2} \frac{\xi_o^2(\xi_o^2-1)}{s_o^{3/2}x^{1/2}}$$

$$\times \left[\{c_2(1+0.85s_c/s_o)^{-1/3} + (1-n_\sigma^2\beta_o^2)^{1/2}(1-n_\sigma^2\beta_o^2\cos^2\theta)^{1/2}\}^2 \right.$$

$$\left. + \frac{n_\sigma^2\beta_o^2 T_\sigma^2 \xi_o \sin^4\theta}{2(s_o+s_c)} \right] (1-n_\sigma^2\beta_o^2\cos^2\theta)\left(1+\frac{a_3 s_c}{3s_o}\right)^{1/6} Z^{2s_o}$$

$$\times \exp[-\mu(\gamma_o-1)], \qquad 29a.$$

where

$$\mu = \frac{mc^2}{k_B T}, \qquad \gamma_o = \left[1+\frac{2\nu}{\mu\nu_B}\left(1+\frac{9x}{2}\right.\right. \qquad ,$$

$$\beta_o = \left(1-\frac{1}{\gamma_o^2}\right)^{1/2}, \qquad x = \frac{\nu}{\nu_B}\frac{\sin^2\theta}{\mu}, \qquad n_\sigma \approx 1-\frac{\nu_p^2}{\nu^2},$$

$$T_o = -T_x^{-1} = -[a+(1+a^2)^{1/2}], \qquad a = \frac{\nu_B}{\nu}\frac{\sin^2\theta}{2\cos\theta},$$

$$s_o = \gamma_o \frac{\nu}{\nu_B}(1-n_\sigma^2\beta_o^2\cos^2\theta), \qquad a_3 = 13.589,$$

$$\xi_o - (1-\beta'^2)^{-1/2}, \qquad \beta' - \frac{n_\sigma\beta_o\sin\theta}{(1-n_\sigma^2\beta_o^2\cos^2\theta)^{1/2}},$$

$$s_c = \frac{3}{2}\xi_o^3, \qquad c_2 = T_\sigma\cos\theta(1-n_\sigma^2\beta_o^2), \qquad Z = \frac{\beta' e^{1/\xi_o}}{1+1/\xi_o},$$

$$\frac{\kappa_\nu B}{N} \approx 507 \sin^6\theta B^{10}\nu^{-10}, \qquad 29b.$$

$$\frac{\eta_\nu}{BN} \approx 1.2 \qquad \nu_B \qquad N \qquad 30.$$

$$r_c \approx 13.1\, T^{-0.138}\, 10^{0.231\cos\theta - 0.219\cos^2\theta} \left(\frac{\nu}{\nu_B}\right)^{-0.782 + 0.545\cos\theta}$$

$$(\tau_\nu \ll 1), \qquad 31.$$

$$\nu_{peak} \approx \begin{cases} 1.4\left(\frac{NL}{B}\right)^{0.1} (\sin\theta)^{0.6} T^{0.7} B & (10^8 < T < 10^9 \text{ K}), \quad 32a. \\ 475\left(\frac{NL}{B}\right)^{0.05} (\sin\theta)^{0.6} T^{0.5} B & (10^7 < T < 10^8 \text{ K}). \quad 32b. \end{cases}$$

An evaluation of the error in Equation 29a was given by Robinson & Melrose (1984). Over a range of more than 12 orders of magnitude, the accuracy is better than 20% for $\nu/\nu_B > 5$, $\theta \gtrsim 10°$, and $T \gtrsim 10^7$ K. The accuracy of Equation 31 for the degree of circular polarization is better than 30%.

Gyrosynchrotron Radiation From Power-Law Electrons

We now consider an electron distribution that is isotropic in pitch angle and power law in energy:

$$n(E) = KE^{-\delta}, \qquad 33.$$

where K is related to N, the number of electrons per cubic centimeter with $E > E_o$, by the relation

$$K = (\delta - 1)E_o^{\delta - 1}N. \qquad 34.$$

For normalization we assume $E_o = 10$ keV $= 1.6 \times 10^{-8}$ erg, but in fact electrons with energy less than 50 to 100 keV contribute very little to the radiation.

Figure 3 shows spectra of the quantities η_ν/BN, $\kappa_\nu B/N$, T_{eff}, and r_c for the x-mode calculated numerically. The slopes of the curves are approximately constant for $\nu/\nu_B \gtrsim 10$, so the spectra can be well approximated by power-law expressions. Empirical expressions (from Dulk & Marsh 1982) for the quantities, valid over the range $2 \lesssim \delta \lesssim 7$, $\theta \gtrsim 20°$, and $10 \lesssim \nu/\nu_B \lesssim 100$,

Figure 3 Characteristics of gyromagnetic emission for the x-mode calculated numerically. (*a–d*) Power-law electrons: Curves are shown for three values of electron power-law index δ and for viewing angles 40° (solid lines) and 80° (dashed lines). The low-energy cutoff in the electron distribution is 10 keV. Shown are (*a*) emission coefficient, (*b*) absorption coefficient, (*c*) effective temperature, and (*d*) degree of circular polarization. (*e–f*) Thermal electrons: Curves of the absorption coefficient (*e*) and degree of circular polarization (*f*) are shown for various electron temperatures and for viewing angles of 40° (solid lines), 80° (dashed lines), and (for r_c) 60° (dot-dash lines).

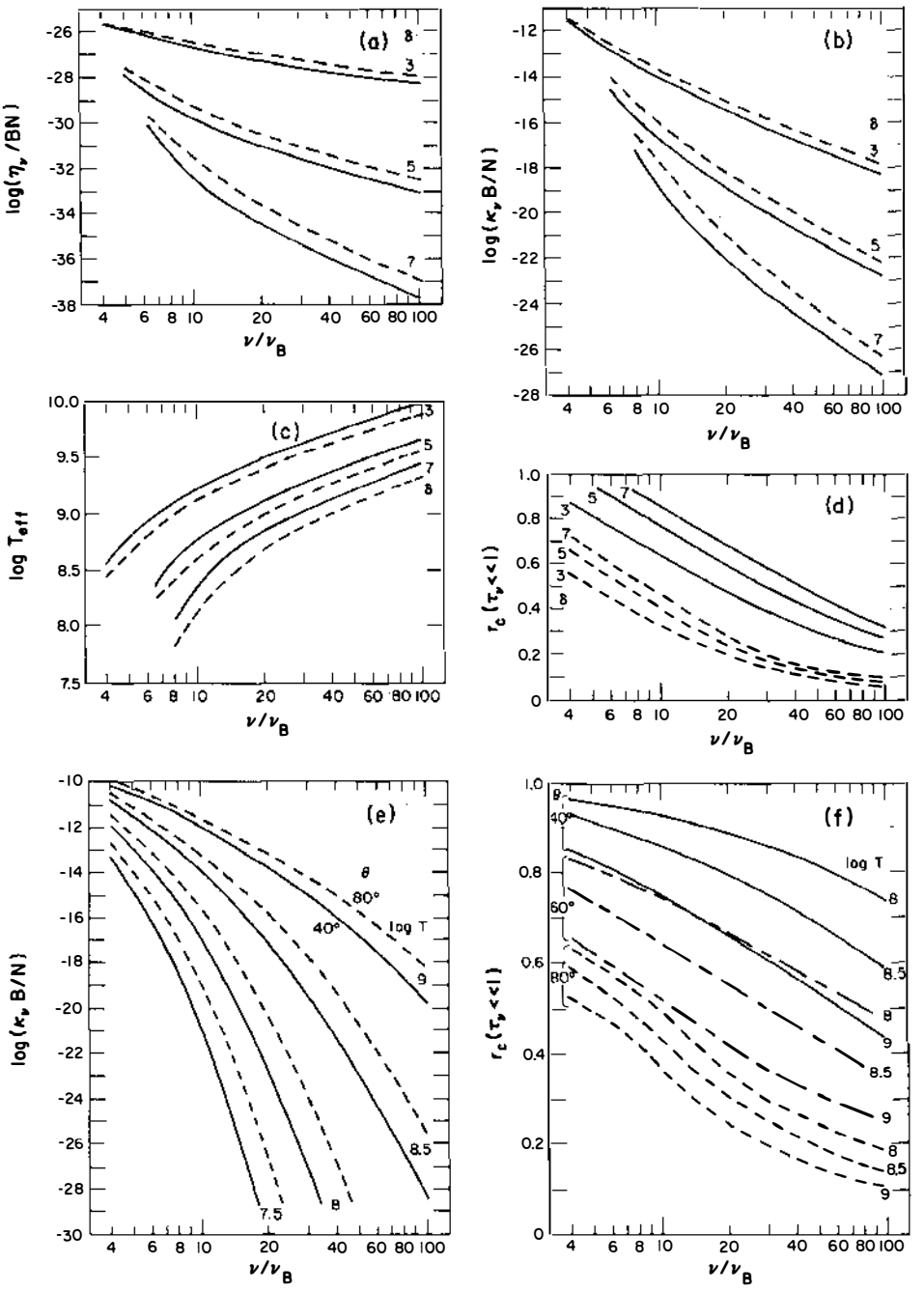

are

$$\frac{\eta_\nu}{BN} \approx 3.3 \times 10^{-24} 10^{-0.52\delta} (\sin\theta)^{-0.43+0.65\delta} \left(\frac{\nu}{\nu_B}\right)^{1.22-0.90\delta}, \quad 35.$$

$$\frac{\kappa_\nu B}{N} \approx 1.4 \times 10^{-9} 10^{-0.22\delta} (\sin\theta)^{-0.09+0.72\delta} \left(\frac{\nu}{\nu_B}\right)^{-1.30-0.98\delta}, \quad 36.$$

$$T_{\rm eff} \approx 2.2 \times 10^{9} 10^{-0.31\delta} (\sin\theta)^{-0.36-0.06\delta} \left(\frac{\nu}{\nu_B}\right)^{0.50+0.085\delta}, \quad 37.$$

$$r_c \approx 1.26\ 10^{0.035\delta} 10^{-0.071\cos\theta} \left(\frac{\nu}{\nu_B}\right)^{-0.782+0.545\cos\theta} \quad (\tau_\nu \ll 1), \quad 38.$$

$$\nu_{\rm peak} \approx 2.72 \times 10^{3} 10^{0.27\delta} (\sin\theta)^{0.41+0.03\delta} (NL)^{0.32-0.03\delta} \times B^{0.68+0.03\delta}. \quad 39.$$

Only the first two of the above equations are independent, for the others are derivable from Equations 35 and 36. However, all are useful because η_ν/BN alone is needed if $\tau \ll 1$, $T_{\rm eff}$ alone if $\tau \gg 1$, and κ_ν/BN or $\nu_{\rm peak}$ alone if $\tau \approx 1$. The accuracy of the expressions has been evaluated by Dulk & Marsh (1982), who find that generally they are good to better than 30%; however, the accuracy worsens at $\delta \gtrsim 6$, especially at large θ and extremes of θ and ν/ν_B. Note, however, that Equations 31 and 38 differ from the equivalent expressions of Dulk & Marsh (1982) because there was an error in the numerical calculations on which their expressions were based.

Synchrotron Radiation From Power-Law Electrons

In the ultrarelativistic limit the angular pattern of the emission is sharply peaked in the direction of an electron's instantaneous motion. The Bessel functions are well approximated by Airy functions. For electrons with a broad range of pitch angles, the emission occurs over a broad band centered on $\nu \approx \nu_B \gamma^2 \sin\theta/2$, i.e. at harmonic numbers $s \approx (\gamma \sin\theta)^3$.

For a distribution of electrons that is isotropic in pitch angle and is power law in energy above E_o, expressions for the emissivity (in each of the o- and x-modes, assumed circularly polarized), for the absorptivity, for effective temperature, and for frequency of peak flux density are, respectively, given by (e.g. Lang 1980)

$$\frac{\eta_\nu}{BN} = \frac{1}{2}(\delta-1)E_o^{\delta-1} g(\delta) \frac{\sqrt{3}e^3}{8\pi mc^2} \sin\theta \left[\frac{2m^2c^4}{3\sin\theta}\frac{\nu}{\nu_B}\right]^{-(\delta-1)/2} \quad 40.$$

$$\approx 8.6 \times 10^{-24}(\delta-1)\sin\theta \left[\frac{0.175}{\sin\theta}\left(\frac{E_o}{1\ \rm MeV}\right)^{-2}\frac{\nu}{\nu_B}\right]^{-(\delta-1)/2},$$

where $g(\delta)$ involves a product of gamma functions and is within 15% of 1.85 over the range $2 \leq \delta \leq 5$;

$$\frac{\kappa_\nu B}{N} = (\delta-1)E_o^{\delta-1}h(\delta)\frac{2\pi e m^5 c^{10}}{9}\frac{1}{\sin\theta}\left[\frac{m^2c^4}{3\sin\theta}\frac{\nu}{\nu_B}\right]^{-(\delta+4)/2} \qquad 41.$$

$$\approx 8.7\times10^{-12}\frac{\delta-1}{\sin\theta}\left(\frac{E_o}{1\text{ MeV}}\right)^{\delta-1}\left[\frac{8.7\times10^{-2}}{\sin\theta}\frac{\nu}{\nu_B}\right]^{-(\delta+4)/2},$$

where $h(\delta)$ is within 15% of 0.74 over the range $2 \leq \delta \leq 5$;

$$T_{\text{eff}} \approx 2.6\times10^9\, 2^{-\delta/2}\left[\frac{\nu}{\nu_B\sin\theta}\right]^{1/2}; \qquad 42.$$

$$\nu_{\text{peak}} \approx 3.2\times10^7\sin\theta\left(\frac{E_o}{1\text{ M}}\right)^{(2\delta-2)/(\delta+4)}$$

$$\times\left[8.7\times10^{-12}\frac{\delta-1}{\sin\theta}NL\right]^{2/(\delta+4)}B^{(\delta+2)/(\delta+4)}. \qquad 43.$$

The degree of linear polarization for a uniform, homogeneous, optically thin source is

$$r_l = (\delta+1)/(\delta+7/3), \qquad 44.$$

and its direction is perpendicular to the field. By using Equation 44 with Equations 41 and 42, expressions can be obtained for the parallel and perpendicular components; the emissivity and brightness temperature of the perpendicular component can be up to twice those given by Equations 41 and 42. The degree of circular polarization of synchrotron radiation is small; expressions are given by Melrose (1971), Lang (1980), and Robinson & Melrose (1985). Of course, if the field in the source region is randomly oriented, both the linear and circular polarization approach zero.

The spectral index at the optically thick low frequencies of a synchrotron spectrum is 2.5, independent of the electron energy index δ, while that at the optically thin high frequencies is (see Figure 2)

$$\alpha = -(\delta-1)/2. \qquad 45.$$

Razin-Tsytovich Suppression

In the presence of a plasma, gyrosynchrotron emission is suppressed (especially at low frequencies) whenever the index of refraction deviates significantly from unity. In the ultrarelativistic limit, suppression occurs at (e.g. Ginzburg & Syrovatskii 1969, Melrose 1980b, p. 100)

$$\nu \lesssim \frac{2\nu_p^2}{3\nu_B\sin\theta}, \qquad 46.$$

while for mildly relativistic electrons it occurs at

$$\nu \lesssim \frac{\nu_p^2}{\nu_B}, \tag{47.}$$

and for nonrelativistic electrons at

$$\nu \lesssim 2\nu_p. \tag{48.}$$

In terms of harmonic numbers, and for non- or mildly relativistic electrons, suppression occurs at

$$s \lesssim \frac{\nu_p^2}{\nu_B^2}. \tag{49.}$$

Electron-Cyclotron Masers

Maser, the predecessor of laser, is the acronym for microwave amplification by stimulated emission of radiation. The class of maser that amplifies radiation at frequencies near the electron-cyclotron frequency and perhaps its low harmonics is the one of interest here. The theory was first investigated by Twiss (1958) and Schneider (1959), but because they utilized an incomplete resonance condition, there were severe difficulties in producing amplified radiation that could escape from a plasma. Only recently did Wu & Lee (1979) utilize the full-resonance condition and show that escaping radiation can arise under much milder conditions than previously thought. The basic requirements for the maser to operate are (*a*) a population inversion in the electron distribution as compared with equilibrium, i.e. a pump for the maser, and (*b*) a relatively strong field or low-density plasma so that $\nu_B \gtrsim \nu_p$; if the latter condition is not met, the free energy is likely to go into various plasma waves rather than directly into electromagnetic radiation.

Although other varieties may sometimes be important, the most common form of population inversion in astrophysical situations is the loss-cone distribution, produced when electrons are energized in magnetic flux tubes that have converging legs and whose footpoints are in a high-density atmosphere. Examples include the field lines of a planetary magnetosphere, the magnetic flux tubes within an active region of the Sun or a flare star, and the field lines connecting the two stars of a close binary pair. Figure 4 is a sketch of a flux tube such as might exist in a stellar atmosphere, one where acceleration or heating is creating a population of energetic electrons. In this situation some fast electrons hit and are absorbed in the high-density atmosphere at the footpoints, while the remainder of the electrons reflect in the converging field, thus creating a loss-cone anisotropy.

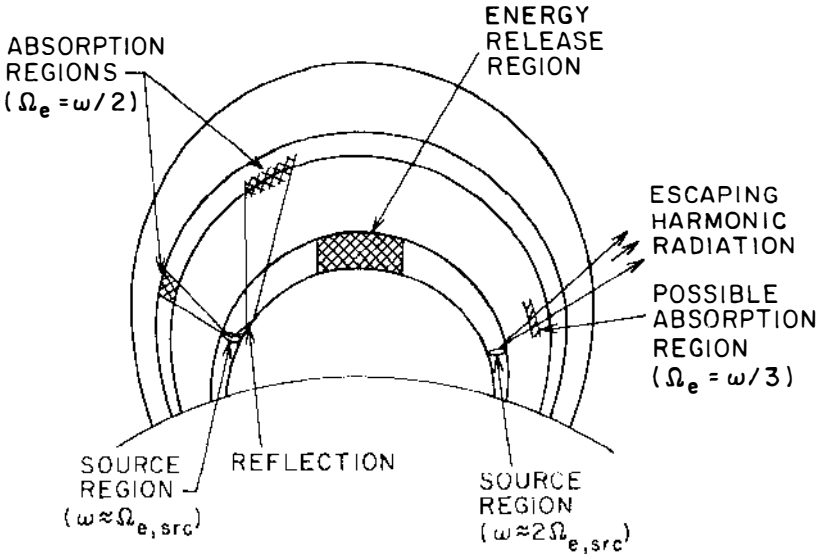

Figure 4 Schematic drawing of a sequence of magnetic flux tubes. At the top of a loop is a region where energy release is occurring. On the left is sketched a maser source region emitting at frequency $\omega = \Omega_c + \Delta$ at a location where the field strength is B_{src}. The cone of radiation is shown, including a reflection of the portion directed toward higher field strength; this radiation is reabsorbed at locations where $B = B_{src}/2$. At the right is sketched a maser operating at $2\Omega_c + \Delta$, perhaps being reabsorbed where $B = 2B_{src}/3$.

The sequence of steps leading to maser radiation have been laid out in a series of papers, e.g. Wu & Lee (1979), Lee et al. (1980), Hewitt et al. (1981, 1982), Melrose & Dulk (1982a), Omidi & Gurnett (1982), Sharma et al. (1982), Hewitt et al. (1983), Melrose et al. (1984), and Winglee (1985). The following summary is based on these works.

1. Acceleration or heating of electrons must occur, presumably as a result of magnetic reconnection, and the electron energy must be divided between a parallel (to the magnetic field) and a perpendicular component. In stellar plasmas there are reasons to expect that the electrons leave the energy release region with an approximately isotropic pitch angle distribution (e.g. Smith & Brown 1980, Grognard 1985), so that on average the two components are about equal; the loss-cone-driven maser, as described below, depends on both components being present, although not necessarily in equal proportion. Other instabilities might arise from other distributions, e.g. the two-stream instability for streaming electrons. Typical energies of the electrons are probably ~ 10 keV to ~ 1 MeV in the conditions of interest.

2. Electrons with small pitch angles α less than a critical value α^* precipitate into the dense atmosphere and are lost. The value of α^* depends on the convergence factor between the top of the flux tube and the footpoints. For a symmetric flux tube, we have

$$\alpha^* = \arcsin (B_{top}/B_{foot})^{1/2}. \quad 50.$$

Typical values of B_{top}/B_{foot} might be 0.1 to 0.5, whence the fraction precipitating becomes 0.05 to 0.3. [For a flux tube of uniform cross section ($\alpha^* = \pi/2$), all electrons precipitate and a maser is impossible.] Meanwhile, the electrons with $\alpha > \alpha^*$ reflect in the converging field in the legs. The resulting electron distribution at typical locations in the legs of the flux tube is sketched in Figure 5; there are few electrons with small, upgoing pitch angles.

At a given location in one leg of the flux tube, the idealized electron distribution in $(v_{\|}, v_{\perp})$ space is sketched in Figure 6, where the semicircular inner contours represent isotropic cold background electrons, and where the deviation from semicircles in the outer contours demonstrates the lack of fast electrons with small pitch angles, i.e. with large $v_{\|}$ and small $v_{\perp}$.

3. The loss-cone anisotropy is the source of the free energy to drive a maser. Consider electrons of energy E_1 at point 1 on Figure 6. If such electrons are induced by a wave to move toward point 2, where $E_2 < E_1$, the electrons will give up some energy to the wave. But for the reverse process, there are few electrons at point 2 that can move to point 1 and absorb energy from the wave. This is opposite to the equilibrium situation, i.e. there is a positive slope in $v_{\perp}$ that can lead to net amplification.

4. Specifically, we consider electromagnetic waves of frequency ω and wave vector $\mathbf{k}$, and electrons with Lorentz factor γ, momentum $\mathbf{p} = \gamma m_e \mathbf{v}$, and with a distribution $f(\mathbf{p})$. Gyroresonance emission and/or absorption occurs when the resonance condition between the electrons and waves is satisfied, i.e. when

$$\omega - s\Omega_e/\gamma - k_{\|} v_{\|} = 0. \quad 51.$$

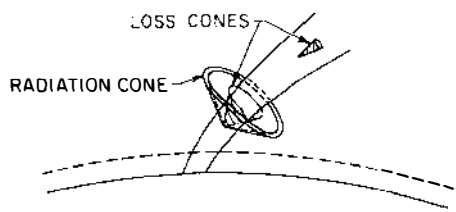

Figure 5 A portion of a loop where energy release is occurring, showing two one-sided loss cones of the electron distribution and a radiation cone in the direction where the maser growth rate is largest.

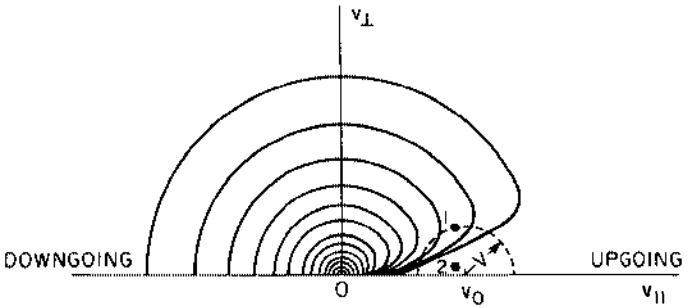

Figure 6 Contour map of the electron distribution in $(v_\parallel, v_\perp)$ space, showing an idealized one-sided loss cone, the dense contours of a possible background component near the center, and (dashed curve) a resonance ellipse that corresponds to a growing electromagnetic wave mode. While giving its perpendicular energy to the wave, an electron at position 1 would move toward position 2 as a result of quasi-linear diffusion, which tends to fill the loss cone.

The special case when $k_\parallel = 0$ or $v_\parallel = 0$ is the one considered by Twiss (1958); radiation is then at $\omega < s\Omega_e$ and cannot escape. However, even if $k_\parallel v_\parallel$ is only a few percent of ω, the emitted radiation can then be higher than $s\Omega_e$ and can escape.

Insight into the maser process can be obtained by considering the location in $(v_\parallel, v_\perp)$ space where the electrons resonantly interact with a wave of given (ω, k) or (equivalently, because of the dispersion relation) of given (ω, θ). With $\gamma = (1 - v_\parallel^2/c^2 - v_\perp^2/c^2)^{-1/2}$, Equation 51 defines an ellipse with major axis parallel to the $v_\perp$-axis. With the nonrelativistic approximation ($\gamma = 1$), the ellipse degenerates into a line (e.g. Hewitt et al. 1981). In this case, extreme anisotropies are needed if wave growth is to occur; this was a major difficulty of maser theories developed before 1979. However, for mildly relativistic electrons of $E \lesssim 500$ keV, a good approximation is $\gamma^{-1} \approx 1 - v_\parallel^2/2c^2 - v_\perp^2/2c^2$, and then Equation 51 defines a semicircle with center

$$v_\parallel/c = k_\parallel c/\omega, \qquad v_\perp = 0 \tag{52.}$$

and with radius

$$\frac{V}{c} = \left(\frac{k_\parallel^2 c^2}{\omega^2} - \frac{2(\omega - s\Omega_e)}{s\Omega_e} \right)^{1/2}. \tag{53.}$$

An example of such a resonant semicircle is shown in Figure 6.

The growth rate of waves in the magnetoionic modes is (e.g. Melrose 1980b, p. 275)

$$\Gamma_s^\sigma(\mathbf{k}) = \int A_s^\sigma(\mathbf{p}, \mathbf{k}) \delta(\omega - s\Omega_e/\gamma - k_\parallel v_\parallel) \left[\frac{s\Omega_e}{\gamma v_\perp} \frac{\partial}{\partial p_\perp} + k_\parallel \frac{\partial}{\partial p_\parallel} \right] f(\mathbf{p})\, d^3\mathbf{p}, \tag{54.}$$

where **p** is the momentum of an electron. A simplified form of A_s is (Melrose & Dulk 1982a)

$$A_s^\sigma(\mathbf{p},\mathbf{k}) \approx \frac{4\pi^2 e^2 c^2 \beta^2 \sin^2\theta}{(1+T_\sigma)^2} \frac{s^{2s}}{2^{2s}(s!)^2} (\beta \sin\theta)^{2s-2}(1+|\cos\theta| T_\sigma)^2, \qquad 55.$$

and T_σ is the axial ratio of the polarization ellipse for mode σ ($\sigma = +1$ and -1 for the o- and x-modes, respectively). With axial symmetry and the resonance condition, the three-dimensional integral in Equation 54 reduces to a one-dimensional integral around the resonance ellipse. At each point on the ellipse, the contribution of the electrons to wave growth is determined by the sign and magnitude of the two terms involving derivatives in Equation 54. Net growth requires that the positive contributions exceed negative contributions. In the semirelativistic approximation, we have $k_\parallel \ll \omega/c$ and $\omega \approx s\Omega_e$, so that the derivative involving $p_\perp$ is much larger than that involving $p_\parallel$. In a loss-cone distribution, there is a deficiency of electrons with small $v_\perp$, and hence we have $\delta f/\delta p_\perp > 0$ at small values of $v_\perp$. Amplification occurs for waves corresponding to resonance semicircles that lie primarily within the loss cone, such as the dashed line in Figure 6. The maximum growth rate occurs for the waves (ω, θ) with the largest (weighted) integrated value of $\delta f/\delta p_\perp$. Amplification occurs at a frequency slightly higher than $s\Omega_e$, and the radiation can escape without passing through the sth harmonic layer, where thermal electrons can produce strong gyroresonance absorption. (Of course, it still must pass through harmonic layers at $s+1$, $s+2$, etc., and absorption may occur there, although generally not as severe.)

5. To estimate the rate of wave growth, we suppose that a loss cone exists for $v > v_{min}$, that it is empty ($f = 0$) for $\alpha < \alpha_o - \delta\alpha$, and that f rises linearly with α over the range $\alpha_o - \delta\alpha < \alpha < \alpha_o$. Also, we assume that outside the loss cone, f is an isotropic power-law distribution $f \approx v^{-a}$ and hence has an energy spectral index $\delta = (a-1)/2$. (Instead of a power law, a Maxwellian distribution with a loss cone would do as well, and the exact form of the loss cone is not critical.) Then the growth rate of a maser whose resonant semicircle is centered at v_o, normalized to the frequency $\omega \approx s\Omega_e$, is (Melrose & Dulk 1982a)

$$\frac{\Gamma_s}{\omega} = \eta_s \frac{n_o}{n_e} \left(\frac{\omega_p}{\omega}\right)^2 \left(\frac{c}{v_o}\right)^2 \left[\frac{v_o}{c} \sin\alpha_o \cos\alpha_o\right]^{2s-2}, \qquad 56.$$

where η_s is a number typically of order unity, α_o was defined above, and

$$n_o = \frac{4\pi}{a-3} (mv_o)^3 f_o \qquad 57.$$

is the number density of electrons with $v > v_o$, i.e. the fast ones that produce the maser radiation (those with $E \gtrsim 10$ keV in solar flares).

The growth rate (Equation 56) depends on v_o as $\Gamma_s \approx v_o^{2s-a-1}$, which [for small $s \leq 2$ and typical values of a (≈ 5 to ≈ 12)] maximizes for the minimum value $v_o = V + v_{min} = v_{min}/(1 - \sin \alpha_o)$. Growth at $s = 2$ is generally less rapid than at $s = 1$, but it is relatively more favorable for electrons with the greatest speeds for which the power law $f \approx v^{-a}$ remains valid.

As an illustration, consider the growth rate for the fundamental ($s = 1$), the x-mode, and a typical loss-cone distribution with $\alpha_o \approx 0.1$ rad. Then with $\omega \approx \Omega_e = 10^{10}$ rad s^{-1}, $\omega_p/\Omega_e = 0.1$, $v_o/c = 0.1$, and $n_o/n_e = 10^{-3}$, we have

$\Gamma_1 \approx 10^7$ s^{-1} or

$\tau_{growth} \approx 10^{-7}$ s or

amplification length ≈ 10 m.

With such a high growth rate, saturation will occur in about $30\tau_{growth}$ or a few microseconds.

6. The bandwidth of an individual pulse of maser radiation is quite small: The range $\Delta\omega$ between frequencies of half-maximum growth rate is $\Delta\omega/\omega \lesssim 0.01$. However, radiation should emanate from electrons at a range of heights along the flux tube and, very likely, from a number of flux tubes in which there is a considerable range of B and Ω_e; thus the overall frequency range of maser emission is likely to be quite large, perhaps 2:1 or more. (It is at least 4:1 in the cases of Earth and Jupiter.)

7. The growth rate is largest at an angle $\theta \approx 70°$ for the x-mode at $s = 1$, and at $\theta \approx 75°$ to $80°$ for other modes and harmonics, i.e. the radiation is directed nearly perpendicular to the field but slightly upward, as sketched in Figure 4. The angular width of the conical sheet of emission of an individual pulse of maser radiation is $\lesssim 1°$, depending somewhat on mode and harmonic. However, different pulses of radiation emanating from electrons of various speeds and pitch angles extend the angular range to $\approx 10°$. Further extensions of the overall range are expected from the curvature of field lines in individual loops and because of reflection of some rays, as shown in Figure 4.

8. Growth rates for various modes and harmonics and their variation with plasma density are illustrated in Figure 7. These are maximum growth rates as functions of ω and θ, calculated by Melrose et al. (1984) for a Maxwellian electron distribution with an idealized loss cone. Growth of the x-mode at $s = 1$ is fastest when the plasma density is low but becomes strongly suppressed at higher densities ($\omega_p/\Omega_e \lesssim 0.3$ to 0.5), with the higher

values applying when the average electron energy in the source region is high (Winglee 1985). The o-mode and z-mode at $s = 1$ are then the fastest growing modes, and these have comparable growth rates until $\omega_p/\Omega_e \approx 1.4$. We expect these results to change somewhat for different electron distributions; in particular, growth of higher harmonics is relatively more favorable if the distribution is weighted toward higher-energy particles, such as in a power-law distribution (e.g. Sharma & Vlahos 1984, Vlahos & Sharma 1984).

9. A major consideration with radiation at $\omega \approx \Omega_e$ is the likelihood of its extracting all of the free energy from the (anisotropic) electron distribution because it is the fastest-growing mode; if so, it may prevent growth at higher harmonics, a point we return to in the next section. In a stellar atmosphere, all radiation at $\omega \approx \Omega_e$ will very likely be absorbed en route from the source

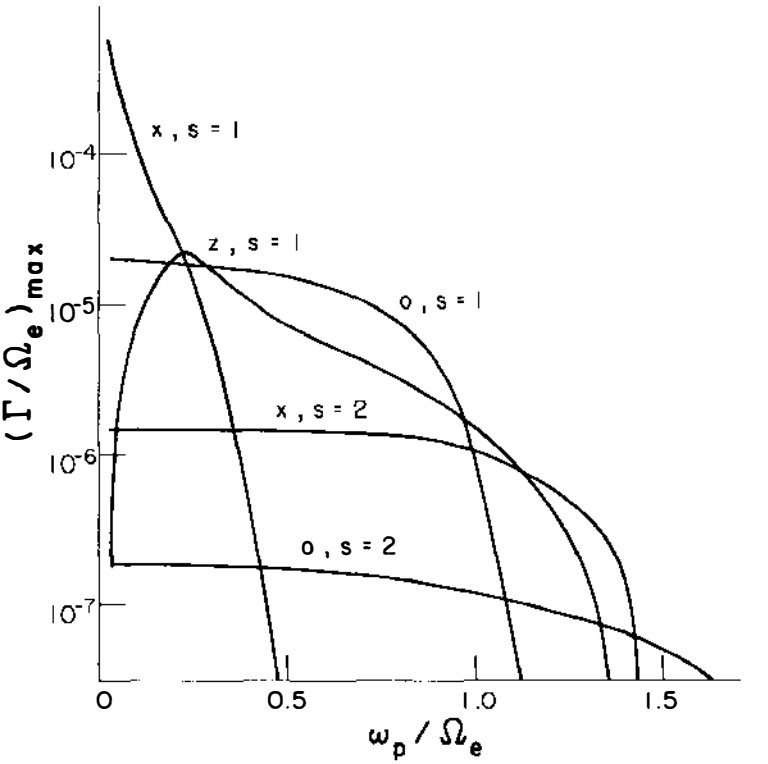

Figure 7 The normalized maser growth rate (maximum as a function of θ and ω) plotted as a function of ω_p/Ω_e for the fundamental ($s = 1$) x-, o-, and z-modes, and for the second harmonic ($s = 2$) x- and o-modes. (From Melrose et al. 1984.)

to the observer. Specifically, gyroresonance absorption by the ambient electrons is very strong at the second harmonic layer, i.e. $\tau \approx 10^4$ at the location between the source and observer where $B = B_{src}/2$ (as sketched in Figure 4). The amount of energy in this radiation is likely to be prodigious— $\sim 10^{27}$ erg s^{-1} for a small solar flare, $\sim 10^{30}$ erg s^{-1} for a large one, and perhaps several orders of magnitude more in a stellar flare. This energy, when reabsorbed, can heat a large volume of ambient plasma to $\sim 10^7$ K, and the heated plasma can then radiate the energy away in the form of soft X rays. Discussion of this RF heating model is beyond the scope of this paper; details can be found in Melrose & Dulk (1982b, 1984).

10. In view of (9.), it seems unlikely that radiation at $s = 1$ can escape from a stellar atmosphere to produce the observed radiation. Holman et al. (1980) suggested that the radiation escapes through a "window" at $\theta = 0°$, but because the radiation is generated at $\theta \approx 70°$, this seems highly improbable. Maser radiation in the o-mode at $s = 1$ is also possible (e.g. Figure 7), but it too is unlikely to escape from a stellar atmosphere because absorption at the second harmonic layer is very strong ($\tau \approx 10^3$).

An alternative is to produce the radiation at a frequency slightly above the second harmonic ($\nu \approx 2\Omega_e$). Such radiation would not suffer gyroresonance absorption at $s = 2$, i.e. near the emission region, and could travel at least to the third harmonic absorption layer, where $B = 2B_{src}/3$. At that layer the optical depth is not negligible ($\tau \gtrsim 10$), and it may require an unusually low ambient density, temperature, or magnetic scale length to allow significant radiation to escape. If so, we may be observing only a small fraction of maser-producing flares.

Three ways have been suggested to produce amplified radiation just above the second harmonic. Melrose & Dulk (1982a) proposed that the radiation is due to maser emission at $\omega \approx 2\Omega_e$, probably produced by the fastest electrons in the distribution and at those locations where the ambient density is high enough to suppress x-mode maser action at $\omega \approx \Omega_e$. The second possibility, proposed by Melrose et al. (1984), invokes amplification of z-mode radiation at $\omega \approx \Omega_e$. As seen in Figure 7, the calculated growth rate for the z-mode is larger than that for most other modes, and it is even more favored when its slow group speed and wide bandwidth for growth are taken into account. The z-mode is nonpropagating, but in theory it is possible to convert a substantial amount of z-mode energy into x-mode radiation at the second harmonic. The third possibility, proposed by Vlahos et al. (1983), involves a streaming distribution of fast electrons, coherent emission of electrostatic waves in the upper hybrid branch, and subsequent coherent conversion of these waves into electromagnetic waves at $\omega \approx 2\Omega_e$. If the hypothesized beams of electrons can be maintained in a stellar atmosphere (and not be destroyed by the two-

stream instability), this process has the advantage that the radiation is directed along the magnetic field and so has a better chance of escaping through the absorption window at $\theta \approx 0°$.

According to present theory it seems unlikely that significant amplification can occur at harmonics greater than 2 because faster growth at $s = 1$ (or possibly $s = 2$) would extract all of the free energy. However, Benson (1982, 1984) has reported cyclotron maser emission from the Earth's magnetosphere and found occasions when intense radiation seems to be present not only at $\omega = \Omega_e$ and $\omega = 2\Omega_e$, but (more controversially) also at $\omega = 3\Omega_e$ and even $\omega = 4\Omega_e$. Obviously the problem of generation of harmonics needs further work.

Plasma Radiation

We turn now to the second kind of coherent radio-emitting process that is important for the Sun and stars: plasma radiation. This occurs at the plasma frequency and its second harmonic, but rarely if ever at higher harmonics. It was shown in an earlier section that gyrosynchrotron emission at harmonic s becomes suppressed in plasmas with $\nu_p \gtrsim \nu_B s^{-1/2}$. As shown in Figure 8, it is likely that $\nu_p \gg \nu_B$ throughout most of the solar atmosphere, and usually electrons are not sufficiently energetic to emit at high harmonics of the gyrofrequency, so that plasma radiation is favored. A wide variety of solar bursts is observed at decimetric and longer wavelengths, most of them due to plasma radiation. For other stars the limited data are consistent with a similar situation: Radiation at the longer wavelengths is probably dominated by plasma emission, and at the shorter wavelengths by gyrosynchrotron emission.

At the shorter wavelengths plasma radiation is increasingly rare. This is because the relevant high-density plasma is blanketed with plasma of lower density in which strong gyroresonance reabsorption occurs if the temperature is high and a magnetic field is present, or if the temperature is low, then by strong free-free absorption. The latter possibility can be seen by assuming that the density decreases away from the plasma level (where $\nu = \nu_p$) with a scale height H. Then, using Equation 21, it follows that the free-free optical thickness of the overlying layer, for fundamental radiation, is

$$\tau \approx 1.5 \times 10^{-17} T^{-3/2} \nu^2 H. \qquad 58.$$

For example, with $T = 10^6$ K and emission at $\nu = \nu_p = 1$ GHz, optical depth unity occurs for $H \approx 700$ km, and at $\nu = \nu_p = 10$ GHz for only $H \approx 7$ km. For radiation at the same frequency but at the second harmonic, the optical thickness is 16 times lower than that given by Equation 58. As a result, second-harmonic radiation is observable at higher frequencies than

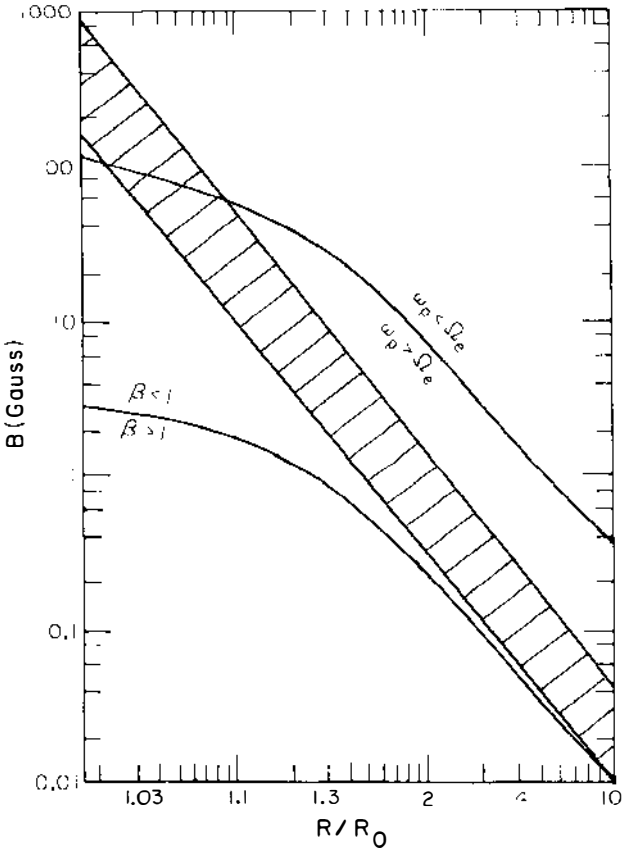

Figure 8 Coronal field strength above an active region, as derived from a number of sources and summarized by Dulk & McLean (1978). The hatched area gives the ranges of field strengths estimated at various heights and includes both observational uncertainty and real variation of field strength among active regions. The curves for $\omega_p = \Omega_e$ and $\beta = 1$, and the relevant altitudes for some of the field strengths, depend on the coronal density model chosen. Here it is a relatively low-density model, twice that of Saito (1970), augmented for low altitudes during flares according to Svestka's (1976) Figure 29.

is fundamental radiation. For the Sun the cutoff frequency above which plasma radiation is strongly reabsorbed is roughly 100–300 MHz for the fundamental and 2–5 GHz for the harmonic.

The theory of plasma radiation is rather more complex than that of the mechanisms discussed earlier because it involves two stages, and one or both may involve plasma instabilities, wave-wave and/or wave-particle interactions, and induced emission. The first stage requires the production of high levels of longitudinal (Langmuir) waves in the plasma, and the

second stage requires some of the Langmuir wave energy to be converted to transverse (electromagnetic) waves that can escape from the plasma and be recorded by a radio telescope. The basic ideas of the present theory were introduced by Ginzburg & Zheleznyakov (1958), but the details have been greatly modified since then. Figure 9 outlines the main features of the

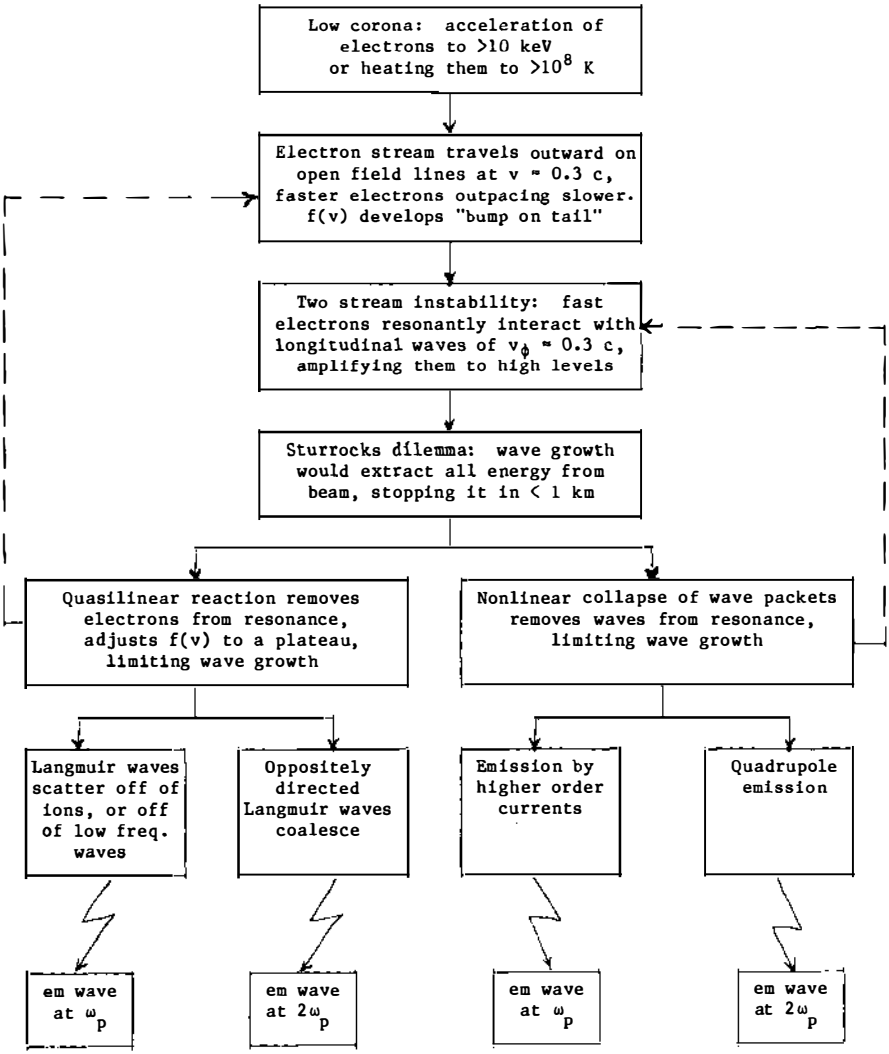

Figure 9 Outline of the plasma emission process associated with a streaming instability (the Type III burst problem).

radiation mechanism, starting with electrons and a streaming instability. Reviews of the recent status are given by Melrose (1980b,c, 1981, 1985a), Goldman (1983), and Grognard (1985). The following synopsis is based on these works.

STAGE 1: PRODUCTION OF LANGMUIR TURBULENCE As with the cyclotron maser instability described above, the generation of high levels of Langmuir waves depends on a source of free energy in the form of a nonequilibrium velocity distribution. However, as discussed by Hewitt & Melrose (1985), it is unlikely that a simple loss-cone anisotropy can lead to an instability for Langmuir waves; in addition, there must be a "gap" in velocity space so that $\partial f/\partial|v|$ is positive for some range of velocities. This distribution is not so easily attained as a simple loss cone.

The only accepted form of anisotropy that can produce high levels of Langmuir waves is the "bump-in-the-tail," or "two-stream," instability outlined in Figure 9. Here the fast electrons are streaming through the plasma, in the x-direction say, so that there is an excess number near the point in velocity space where $(v_x, v_y, v_z) = (v_0, 0, 0)$. The one-dimensional electron distribution $f_1(v)$ obtained by integrating over v_y and v_z can have a positive slope at $v \lesssim v_0$; a proviso here is that v_0 be sufficiently larger than the background thermal speed $V_e = (kT/m)^{1/2}$ to ensure that there is a negligible number of ambient electrons (whose distribution has a negative slope) with $v \approx v_0$. Typically for solar bursts, we have $v_0 \approx 0.1c$ to $0.5c$ or $v_0/V_e \approx 10$ to 50.

There is only one widely accepted means of creating this kind of bump-in-the-tail distribution: by having fast electrons outpace slow ones so that, at some distance from the acceleration region, fast electrons arrive first. In addition, the fast electrons must not be too widely spread in pitch angle, else the bump does not form. For solar Type III bursts the bump forms for electrons of $v \approx 0.1c$ as they stream away from the Sun; faster electrons are too widely spread in pitch angle to form a bump (Lin et al. 1981). Another possible means of creating a bump (or at least a part of velocity space where $\partial f/\partial|v| > 0$) is by a preferential depletion of the lower-speed electrons by collisions within a background plasma.

In the case of interest, where $\omega_p \gg \Omega_e$, a wave mode that can resonantly interact with electrons of $v \lesssim v_0$ and remove the free energy is the Langmuir wave. Its dispersion relation, in terms of phase speed v_ϕ, is

$$v_\phi^2 = \omega^2/k^2 = \omega_p^2/k^2 + 3V_e^2. \qquad 59.$$

Because the wave numbers of Langmuir waves are restricted to less than the inverse of the Debye length λ_D, i.e. $k \lesssim \lambda_D^{-1} = \omega_p/V_e$, Equation 59 implies that $v_\phi^2 \gtrsim 4V_e^2$. The waves that resonantly interact with electrons of $v \lesssim v_0$

are those of $v_\phi \lesssim v_o$, and for these the growth rate is

$$\gamma \approx \frac{n_1}{n_e} \pi \omega_p v^2 \left. \frac{\partial f_1(v)}{\partial v} \right|_{v=\omega/k<v_o}, \quad 60.$$

where n_1 and n_e are the number densities of electrons in the bump and of ambient electrons, respectively. This growth time is short, typically some hundreds of Langmuir periods for the case of streaming electrons and 10^4–10^5 Langmuir periods for loss-cone electrons with a gap.

Growth of Langmuir waves occurs until it is limited or saturated owing to one of several effects: (*a*) The stream may pass or otherwise change its characteristics to destroy the resonance. (*b*) The growing waves may be scattered in angle or altered in $|k|$ to destroy the resonance. Possible means of accomplishing this are scattering off of ions, low-frequency waves or density inhomogeneities, or possibly nonlinear collapse of wave packets into solitons. (*c*) The wave level can saturate by quasi-linear diffusion, i.e. the waves may reach such a high level that they react on the streaming electrons, diffusing them in velocity space so as to remove the positive slope. It is not certain which of these processes is the relevant one for solar bursts; two are indicated in Figure 9.

Whatever the growth-limiting process, it is possible to estimate the saturated energy density in the Langmuir waves (W_L), or equivalently the effective temperature of the Langmuir waves (T_L), defined by

$$W_L = \int \frac{k_B T_L}{(2\pi)^3} d^3\mathbf{k}, \quad 61.$$

where k_B is Boltzmann's constant. An approximation for Equation 61 is

$$k_B T_L = 2\pi^2 W_L \left(\frac{v_o}{\omega_p}\right)^3. \quad 62.$$

Several studies have shown that the saturated value of W_L is $\sim 10^{-5}$ times the energy density of the background plasma, i.e. $\approx 10^{-5} n k_B T$. Hence the limiting value of T_L is of order

$$T_L \approx 10^8 \frac{v_o^2}{c^2} \frac{v_o}{\omega_p} T, \quad 63.$$

which is $\lesssim 10^{15}$ K in circumstances of interest on the Sun.

STAGE 2: PRODUCTION OF RADIO WAVES

A. Fundamental radiation Several ways of converting Langmuir wave energy into electromagnetic waves have been proposed (e.g. Figure 9). In order for conversion to occur with reasonable efficiency, it is necessary that

there be frequency matching

$$\omega_t = \omega_L + \omega_3 \qquad 64.$$

and momentum matching

$$\mathbf{k}_t = \mathbf{k}_L + \mathbf{k}_3, \qquad 65.$$

where subscripts t, L, and 3 represent transverse waves, Langmuir waves, and some third wave or influence, respectively. For fundamental radiation we have $\omega_t \approx \omega_L \approx \omega_p$, so that ω_3 must be small, e.g. a low-frequency wave or a low-frequency fluctuation of the electric field produced by a thermal ion. Also, since $|k_t| \ll |k_L|$, it is required that $\mathbf{k}_3 \approx -\mathbf{k}_L$.

There are three ways by which these relationships might be satisfied and thus give rise to fundamental plasma radiation: (*a*) Scattering by the electric field associated with thermal ions, as originally proposed by Ginzburg & Zheleznyakov (1958). This process is not very efficient; such inefficiency, along with other difficulties, makes it unlikely that it could produce radio brightness temperatures as high as are observed. (*b*) Scattering by low-frequency waves such as ion-sound, lower hybrid, etc. Here the low-frequency turbulence acts like a collection of ions acting coherently, so the efficiency of conversion is enhanced in proportion to the level of the turbulence above the thermal level. In principle, if the low-frequency wave level is nonthermal (as is known to be true within the source regions of some solar bursts), this can give rise to bright radio bursts limited to $T_b = T_L$, i.e. radio brightness temperatures equal to the effective temperatures of the Langmuir turbulence (up to $\sim 10^{15}$ K). In addition, there is a related process in which a Langmuir wave is induced to decay into an ion-sound plus an electromagnetic wave, thus leading to amplification and again to $T_b = T_L$ (Melrose 1980c). (*c*) Direct conversion in the presence of inhomogeneities with sharp density gradients. For this conversion to be efficient, there must be significant density variations on scales of 10 to 100 km; however, the existence of such variations is uncertain.

The polarization of fundamental radio waves produced by any of these processes is predicted to be quite high ($\approx 100\%$) and in the sense of the o-mode. This is because the emitted frequency is below the x-mode cutoff ($\omega_x \approx \omega_p + \Omega_e/2$), and hence no x-mode radiation is emitted. Some types of solar bursts that are known to be at the fundamental and in the o-mode are indeed observed to be nearly 100% polarized, but other types are only partially ($< 50\%$) polarized. The cause of the depolarization for these bursts is not known.

B. Second harmonic radiation For harmonic radiation, it follows that $\omega_t \approx 2\omega_p$ and $k_t \approx \sqrt{3}\omega_p/c$. To obtain frequency matching, it is necessary that $\omega_3 \approx \omega_p$, which leads to the idea that two Langmuir waves coalesce to

produce a radio wave. For momentum matching, since $|k_L| \approx \omega_p/v_o \gg |k_t|$, it is necessary that $\mathbf{k}_L \approx -\mathbf{k}_3$. But the direction of $\mathbf{k}_L$ is approximately along the electron streaming direction, so for the coalescence to work there must be a way to obtain a secondary Langmuir wave distribution that is approximately isotropic or in the backward direction. Such a secondary distribution might be produced by scattering of primary Langmuir waves off of thermal ions or low-frequency waves, but at present the details are uncertain. Nevertheless, given the secondary distribution, the brightness temperature of resulting radio waves can grow to equal the effective temperature of the Langmuir turbulence ($T_b \approx T_L$).

The sense and degree of polarization of radio waves at the second harmonic depend on the angular distribution of the Langmuir waves (Melrose et al. 1980). For highly collimated (forward plus backward) Langmuir waves, the polarization is calculated to be in the sense of the o-mode and with a degree

$$r_c = \frac{11}{48}\frac{\Omega_e}{\omega_p} \qquad (\omega_p \gg \Omega_e). \tag{66.}$$

In the other extreme of isotropic Langmuir waves, the polarization is calculated to be in the sense of the x-mode and with a degree

$$r_c = \frac{85}{48}\frac{\Omega_e}{\omega_p}|\cos\theta| \qquad (\omega_p \gg \Omega_e). \tag{67.}$$

The calculated sense of polarization agrees with observations of solar bursts known to be at the harmonic. However, using Equations 66 and 67, the observed degree of polarization ($r_c \approx 0.1$–0.2) implies field strengths that are higher than one expects to be present according to other (indirect) evidence. Hence, the present state of the theory of plasma-radiation polarization does not seem to be complete.

An alternative mechanism may be important for converting Langmuir wave energy to electromagnetic energy if nonlinear collapse into solitons is the relevant growth-limiting process for Langmuir waves. It has been shown that both fundamental and harmonic radiation can be generated during the collapse (e.g. Goldman 1983), but present theory does not allow the radiated power or wave polarization to be estimated.

In summary, the theory of plasma radiation is not in a completely satisfactory state, despite the immense effort and large number of important achievements in recent years. There is only one known electron distribution, the bump in the tail, that is capable of producing the high levels of Langmuir waves that must exist. Further, the way of attaining the bump in the tail is known for only one (Type III) of several types of solar bursts

whose origin is plasma radiation. Even for Type III bursts, it is not certain whether the Langmuir turbulence is due to quasi-linear or nonlinear effects, and for these bursts there is the enormous advantage of having in situ measurements of plasma and wave parameters within the source regions in the solar wind.

For the conversion of Langmuir wave energy to electromagnetic energy there are several possible mechanisms, and it is not clear which is the relevant one. Fortunately, the theory predicts that brightness temperatures of both fundamental and second-harmonic radiation can reach the effective temperatures of the Langmuir waves, and that brightness temperatures of 10^{15} K or more are achievable. For solar bursts, $T_b \approx 10^{15}$ K is occasionally observed at kilometer wavelengths, 10^{10}–10^{13} K at decameter wavelengths, and 10^{8}–10^{11} K at meter wavelengths.

3. SOLAR RADIO EMISSION

In this section we briefly review various solar radio emissions, many of which are likely to have counterparts on other stars. A number of review articles and books have been written on this subject, notably Wild et al. (1963), Kundu (1965, 1983), Svestka (1976), Krüger (1979), Melrose (1980b,c), and Kundu & Gergely (1980). The most recent and extensive reviews of various aspects of solar radiophysics are contained in the book edited by McLean & Labrum (1985).

Observations of solar radio bursts have been mainly of two kinds: (*a*) Measurements of burst spectra are made with dynamic spectrographs at frequencies $\nu \lesssim 1$ GHz and by single-frequency radiometers at $\nu \gtrsim 1$ GHz. Normally the radiation from the whole Sun is received, so that multiple or moving sources, if they exist, cannot be identified. (*b*) Measurements of source position, structure, size, and polarization are made with imaging instruments such as radioheliographs (Clark Lake, Culgoora, Nancay) and synthesis instruments (Westerbork, VLA). Other valuable data have come from spectrographic polarimeters and separated spacecraft.

A basic characteristic of solar radio emission is that the higher frequencies arise from closer to the solar surface. For the most part this is because emission of a given frequency ν can arise only from regions where the electron plasma frequency ν_p is equal to or lower than ν. Thus, because n_e decreases as a function of height in the solar atmosphere, ν_p also decreases with height, and the lower frequencies must thus arise from greater heights. If, as frequently happens, a disturbance travels outward from the Sun and at each height generates radiation at the local plasma frequency, then the disturbance will create a "dynamic radio spectrum" in which the emission drifts from high to low frequencies at a rate that depends

on the speed of the disturbance and whether the radiation is generated at the fundamental ($\nu = \nu_p$) or second harmonic ($\nu = 2\nu_p$). Many radio bursts are, in fact, generated at frequencies near the plasma frequency or its harmonic, and thus they come from a relatively thin layer above the "plasma level," i.e. above the height where $\nu_p = \nu$. Exceptions are bursts at centimeter wavelengths (which occur in the corona, whereas the plasma level is in the chromosphere) and moving Type IV bursts (where the sources move outward to several solar radii).

Radio Emission From the Quiet Sun

Before turning to the radiation from solar outbursts, we briefly describe the quiescent radio emission. The appearance of the Sun depends on the frequency at which the observations are made. At frequencies $\gtrsim 10$ GHz, the Sun is basically a uniform disk of $T_b \lesssim 1.5 \times 10^4$ K on which are superimposed brighter areas that correspond to active regions. At lower frequencies, the brightness of the disk component increases slowly and that of the active regions rapidly; at $\nu \approx 1$ GHz the disk component has $T_b \approx 5 \times 10^4$ K, the active regions have 1–2 $\times 10^6$ K, and dark regions have appeared that are coronal holes with $T_b \approx 3 \times 10^4$ K. At yet lower frequencies, the disk becomes brighter while the active regions become slightly less bright until at $\lesssim 100$ MHz the entire Sun has $T_b \approx 1 \times 10^6$ K. Then the active regions are no longer distinguishable, the brightest features correspond to coronal streamers, the coronal holes may or may not be slightly less bright than average, and the size of the disk is larger than the optical disk by up to $\approx 50\%$.

Figure 10 shows the appearance of the Sun at 1.4 GHz and compares it with the 1.4-GHz polarization, the brightness distribution in the light of He λ10830 Å, and a magnetogram. The appearance is strongly reminiscent of soft X-ray pictures, with both bright and dark features being present. The bright areas form two bands parallel to the solar equator (the active region belts). The brightest features, individual active regions or combinations, have T_b ranging from about 1 to 2.2 $\times 10^6$ K. Away from active regions are unresolved structures, probably magnetic loops, with $T_b < 1 \times 10^5$ K, and dark regions that are coronal holes and filament cavities.

In the He λ10830 Å image, both active regions and filaments appear dark, while coronal holes and other regions of low-density corona appear bright. Comparing the 1.4-GHz brightness distribution with that in helium and with the magnetogram, and taking into account the poorer resolution of the radio map ($\approx 40''$ vs. $\approx 2''$), we see generally excellent correspondence: (*a*) Active regions, sites of strong magnetic fields, are prominent on each. (*b*) The brighter parts of the quiet regions at 1.4 GHz correspond well to the darker regions in helium and to magnetic regions of mixed polarity and

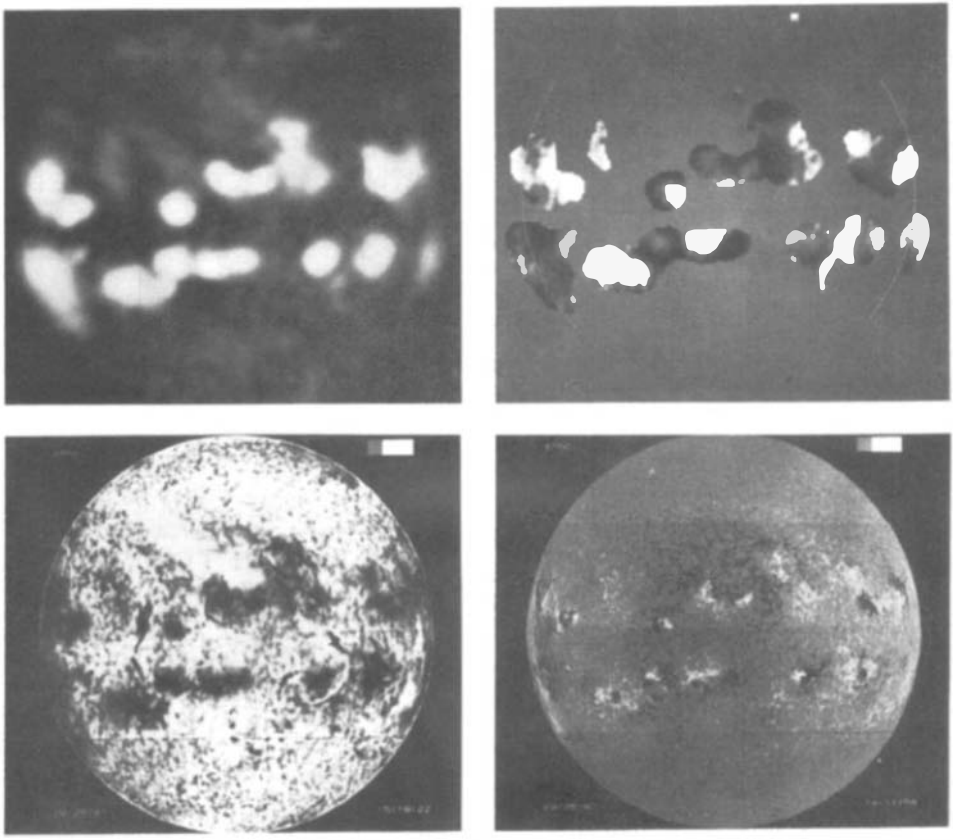

Figure 10 The Sun as observed with the VLA on 1981 September 26, near the peak of the sunspot cycle. (*Upper left*) Intensity at 1.4 GHz, with shading from black to white indicating values of T_b ranging from 0 to 2.2×10^6 K. (*Upper right*) Degree of circular polarization r_c at 1.4 GHz. Dark and light regions represent LH and RH polarization (− and + fields), respectively. The range from black to white represents $-0.22 < r_c < 0.21$. (*Lower left*) Intensity in He λ10830 Å recorded at Kitt Peak National Observatory. (*Lower right*) Magnetogram of the longitudinal component of the photospheric field recorded at Kitt Peak. (From Dulk & Gary 1983.)

moderate strength. (*c*) The large coronal hole in the northeast quadrant is the brightest feature in helium, a region of fairly strong and unipolar magnetic field, and a moderately dark feature at 1.4 GHz. (*d*) Filaments seen in helium correspond to locations of magnetic polarity reversal and to dark voids at 1.4 GHz. (*e*) Extended bright areas in helium (e.g. in the northwest quadrant) correspond to regions of weak field and mixed polarity on the magnetogram and to quite dark areas at 1.4 GHz.

If we compare the 1.4-GHz polarization map with the magnetogram, there is generally close correspondence. The sense of circular polarization corresponds to the x-mode, with LH and RH indicating fields directed away from (negative; black) and toward (positive; white) the observer. Most of the active regions are bipolar, with the brightest radiation located near the line of polarization reversal. The general agreement is somewhat surprising, because the magnetogram represents the photospheric field, while the 1.4-GHz polarization reflects fields in the low corona at heights between ≈ 10 and ≈ 50 Mm.

All of the 1.4-GHz radiation is probably due to free-free bremsstrahlung. Away from active regions the corona is optically thin, and so the brightness has two contributions, one from the corona whose magnitude depends on the coronal density and temperature, and the second from the transition region (especially from the height where $\tau \approx 1$). In coronal holes the coronal contribution is negligible, in quiet regions it is substantial, and in active regions it is dominant. The optical depth of the corona is greater than unity near the cores of active regions and of order unity in the outer parts. The polarization is everywhere $\lesssim 20\%$ and is due to a slightly larger optical depth in the x-mode than the o-mode (see Equation 22).

At frequencies higher than 1.4 GHz, e.g. 5 GHz, the brightness of active regions is mostly lower than 10^6 K because their optical thicknesses are less than unity, but there are often small, bright features with high ($>50\%$) polarization. These features are probably due to gyroresonance emission at harmonic number ≈ 3 (field strengths ≈ 1000 G) making particular parts of active regions optically thick. Such features are not visible at 1.4 GHz, probably because of free-free absorption in the plasma overlying the gyroresonance regions, i.e. the plasma is optically thick.

Metric and Longer Wavelength Bursts

Figure 11 is a schematic diagram of an idealized dynamic spectrum of the kind frequently produced by large flares. Individual events may vary greatly from this idealized spectrum, having one or more components weak or missing altogether. The nomenclature for the various continuum components is often confusing; historically, this situation arose from the fact that spectrographic information alone could not distinguish among the several physical processes that are now known to produce continuum radiation. Alternate names for some components are given in the figure caption.

We now consider the various types of bursts that are observed at meter and longer wavelengths, i.e. at $\nu \lesssim 300$ MHz.

Type I bursts and storms are the most commonly observed radio phenomena of the Sun (e.g. review by Kai et al. 1985). Myriads of Type I

bursts, each lasting about a second, are superimposed upon a continuum that may last for anything from a few hours (following flares, and then designated "Storm continuum") to days or weeks if associated with an intense active region containing a large sunspot (then designated "Type I Storm"). The radiation is usually highly circularly polarized ($>90\%$), but it is sometimes lower ($<50\%$) when the source region is near the limb. These and other characteristics are summarized in Table 1. Theories of Type I storms suggest that Langmuir waves, in the presence of low-frequency waves, produce the observed radio emission at the fundamental plasma frequency. The frequency extent of Type I storms, about 50 to 300 MHz, suggests that the radiation arises in closed-field regions of the low corona, at heights $\lesssim 0.5\ R_\odot$. The greatest uncertainty in the theory is the origin of the required high levels of Langmuir and low-frequency waves.

In association with Type I storms at $\nu \gtrsim 50$ MHz, there often are Type III storms at $\nu \lesssim 50$ MHz. Here there are myriads of Type III bursts superimposed on a continuum background. The observations suggest that electrons are accelerated to $E \approx 5$ keV at fairly great heights ($\approx 0.5\ R_\odot$) and travel outward along open field lines. The radio waves are often observed on spacecraft, occasionally to frequencies as low as 30 kHz (i.e. near 1 AU), and the keV electrons have also been observed by spacecraft near the Earth's orbit.

Type II bursts are very important as indicators of shock waves traveling

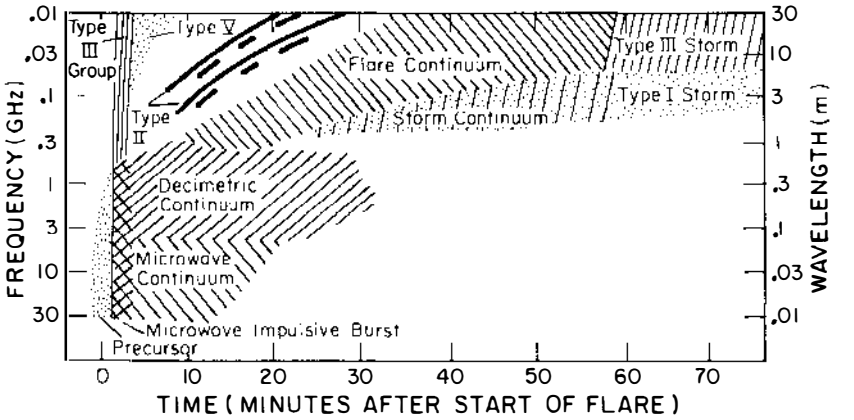

Figure 11 Schematic dynamic spectrum of a solar radio outburst such as might be produced by a large flare. Outbursts often vary considerably from this "typical spectrum." Alternate names for some components are as follows: microwave continuum = Type IVμ, postburst, gradual rise and fall; decimetric continuum = Type IVdm; flare continuum = IVmA, Moving Type IV (if motion is observed); storm continuum = IVmB, Type I storm, noise storm, stationary Type IV; Type III storm = decametric continuum.

Table 1 Summary of the major characteristics of various kinds of solar bursts

Burst type	Duration at 100 MHz or 10 GHz	T_b (K)	Polarization (circular)	Frequency range/ bandwidth	Height range/ magnetic topology	Association	Emission mechanisms
I	$\lesssim$1 s	$\gtrsim 10^{10}$	50–100%	50–300 MHz/ $\simeq$1 MHz (burst)	0.1–0.6 $R_\odot$ closed	large sunspots	fundamental plasma
I storm	days to weeks	$\gtrsim 10^{9}$	o-mode	$\approx$100 MHz (storm)			
III storm	days to weeks	$\gtrsim 10^{9}$	o-mode	50 MHz–30 kHz	0.6 $R_\odot$–1 AU open	I storms	fundamental and/or harmonic plasma
II	$\gtrsim$10 min	10^{8}–10^{11}	usually unpolarized	200 → 1 MHz/ 10 MHz	0.2 → 200 $R_\odot$ open	flare shock wave	fundamental and harmonic plasma
III	few seconds	10^{8}–10^{12} (to 10^{15} at $\sim$1 MHz)	fundamental: 30% harmonic: 10% o-mode	200 → 1 MHz/ 10 MHz 2 harmonics	0.2 → 200 $R_\odot$ open (closed for U or J)	$c/3$ electron stream	fundamental and harmonic plasma
IV moving	$\approx$30 min	10^{8}–10^{9}	low → high x-mode	200–10 MHz/ >10 MHz	0.5 → few $R_\odot$ plasmoid	small flare	gyrosynchrotron and/or plasma
IV flare continuum	$\approx$20 min	10^{8}–10^{12}	0–40% o-mode?	200–10 MHz/ 100 MHz	0.1–1 $R_\odot$ closed?	moderate to large flare, initial phase	plasma?
IV storm continuum	few hours	$>10^{9}$	60–100% o-mode	50–300 MHz/ 100 MHz	0.1–0.6 $R_\odot$ closed?	flare, late phase	fundamental plasma
V	>1 min	10^{8}–10^{11}	<10% x-mode	100 → 10 MHz/ 50 MHz	0.5–2 $R_\odot$ open?	follows some IIIs	harmonic plasma
microwave impulsive	>1 min (at 10 GHz)	10^{7}–10^{9}	$\approx$30% x-mode	3–30 GHz/ 10 GHz	$\approx 10^{4}$ km closed	small to large flares, hard X rays	gyrosynchrotron (Maxwellian or power law)
microwave IV	$\approx$10 min	10^{7}–10^{9}	$\approx$10% x-mode	1–30 GHz/ 10 GHz	10^{4}–10^{5} km closed	large flares with shocks	gyrosynchrotron (power law)
microwave postburst	minutes to hours	$\approx 10^{7}$	low	1–10 GHz/ 5 GHz	10^{4}–10^{5} km closed	flare, late phase	thermal bremsstrahlung
microwave spike burst	$\approx$10 ms (burst) $\approx$10 min (group)	$>10^{13}$	$\approx$100% x-mode?	$\approx$0.5–5 GHz/ few MHz	10^{4}–10^{5} km closed	flare, hard X rays	cyclotron maser

outward through the corona, in some cases to and beyond 1 AU (e.g. reviews by Bougeret 1985, Melrose & Nelson 1985). Their characteristics are given in Table I and illustrated in Figure 11. The radio emission is generated at the fundamental and second harmonic of the local plasma frequency, but the details of the emission mechanism are not known. Presumably there are shock waves that accelerate electrons to a few keV or more; these electrons develop an anisotropy that is unstable to the production of Langmuir waves, and some of the Langmuir wave energy is converted to radio waves. For some bursts there is evidence of electrons streaming away from the shock, but in most cases there is not.

Shocks and/or Type II bursts may be associated with second-phase acceleration of particles to high energies, i.e. ≈ 1 GeV for protons and ≈ 10 MeV for electrons. Fermi acceleration, either directly by the shock or by shock-induced turbulence, is the favored mechanism. Gamma rays are observed within seconds of hard X-ray bursts (the latter are presumably due to first-phase acceleration), which demonstrates that further acceleration must occur very rapidly. Type II (and/or Type IV) bursts are good indicators of mass-ejection transients. For example, almost all Type II (and/or IV) bursts originating within 45° of the limb during the years of low solar activity in 1973–1974 were accompanied by coronal transients observed in white light, and conversely all of the coronal transients whose speed exceeded 500 km s^{-1} produced Type II (and/or IV) bursts. However, more recent observations near solar maximum, when flares are quite frequent, show that this one-to-one relationship does not always hold.

Type III bursts are, after Type I's, the most common kind of solar bursts (e.g. review by Suzuki & Dulk 1985). In moderately active years, some tens of thousands occur. Groups of bursts are common, with various groups containing from 1 to 20 or more individual bursts. Although Type III bursts originate almost exclusively from active regions, most occur without reported flares or subflares. Frequently, as sketched in Figure 11, a large group of Type III bursts occurs at the start of flares. However, more than 90% of Type III bursts occur in the absence of flares, and some 70% of X-ray flares occur without Type III bursts.

Classical Type III bursts begin at a frequency of a few hundred megahertz and drift rapidly to frequencies so low that they can be observed only from space, e.g. 30 kHz or less (see Table 1). Emission can sometimes be observed at both the fundamental and second harmonic of the plasma frequency, although at the higher frequencies ($\gtrsim 100$ MHz) it seems that harmonic radiation only is usually present. Fundamental components are moderately polarized ($\approx 30\%$), while harmonic components are slightly polarized ($\approx 12\%$), both in the sense of the o-mode.

Classical Type III bursts are not the only variety that is observed. Some

have the form of inverted U's, indicating that the electron stream travels up one leg of a coronal magnetic loop and down the other. Others have the form of inverted J's, indicating a similar situation to the U bursts except that the radiation (or stream) stops near the top of the loop. Others, termed "peculiar Type III," have a variety of forms and may appear only at high frequencies or over only a limited frequency range.

Type III bursts are caused by subrelativistic (~ 1 to ~ 50 keV) electron streams traveling outward from the Sun at a speed of about $0.1c$ to $0.5c$. At positions distant from the acceleration region, the fast electrons have outpaced the slow, giving rise to the "bump-in-the-tail" instability. The electrons thus generate high levels of Langmuir waves, and these in turn are converted partly into radio waves. All components—electrons, Langmuir waves, and radio waves—have now been observed by spacecraft. However, there is no agreement on the details of the radiation mechanism, with both quasi-linear and nonlinear theories being proposed. Very likely, there has been more plasma theory developed toward the understanding of Type III bursts than for any other problem in astrophysics (e.g. Goldman 1983, Grognard 1985).

Type IV bursts are of several varieties (see Figure 11 and Table 1). The original definition of Type IV involved an outwardly moving source of continuum radiation, the *moving Type IV*. To detect such motion requires more than a spectrograph, i.e. an interferometer or radioheliograph. It is found that moving Type IV's are quite rare bursts. (Only about three dozen were observed by the Culgoora radioheliograph during a solar cycle.) As reviewed by Stewart (1985), the evidence suggests that most moving sources consist of a self-contained magnetic structure, a plasmoid, in which fast electrons are trapped and emit either plasma or gyrosynchrotron radiation. The evidence for plasma radiation includes the very high brightness temperatures (sometimes $> 10^{10}$ K) and low polarization that are observed early in the source lifetime, and their association with high-density volumes of ejected material within coronal transients. The evidence for gyrosynchrotron radiation includes the high degrees of circular polarization observed late in the lifetime of bursts traveling several solar radii, at times when the brightness temperature is $\lesssim 10^8$ K and decreasing. The most likely explanation is that bright bursts with low polarization and short lifetimes are entirely due to plasma radiation, those with moderate brightness and increasing polarization are the result of gyrosynchrotron radiation, and for some there is a transition from plasma to gyrosynchrotron radiation at some stage in the life of the source.

The *flare continuum* variety of Type IV bursts is much more common than the moving Type IV (e.g. review by Robinson 1985). Flare continuum sources are stationary, with the lower-frequency radiation coming from

greater heights (see Table 1). In most cases the flare continuum starts near the time and frequency of Type II bursts; however, sometimes it starts early in a flare, near the impulsive phase. Brightness temperatures of 10^{12} K or higher are sometimes observed, usually with low-to-moderate circular polarization ($\lesssim 50\%$). It seems likely that the flare continuum is due to plasma radiation from electrons trapped in large magnetic loops in the corona. In order to develop the very high levels of Langmuir waves needed (effective temperatures $> 10^{12}$ K), an unstable electron distribution must exist in the source region. An anisotropy in pitch angle and a "gap" in velocity space seem to be required.

The *storm continuum* variety of Type IV bursts also commonly occurs with moderate to large flares (e.g. review by Kai et al. 1985). It usually starts at frequencies of ≈ 300 MHz within about 10 min of the onset of flares and then drifts to lower frequencies, to about 50 MHz, over the course of an hour or so. On spectropolarimeters the storm continuum radiation is usually distinctly different from the flare continuum because its polarization is much higher ($\gtrsim 50\%$). As discussed above, the total duration is normally a few hours, but sometimes the radiation continues for days and is termed a Type I storm. The inferred radiation mechanism for the storm continuum is fundamental plasma radiation, the same as for Type I.

Type V bursts consist of continuum radiation lasting from one to a few minutes following some Type III bursts or burst groups (e.g. review by Suzuki & Dulk 1985). An important characteristic of the radiation is the evolution from one sense of polarization in the Type III to the other in the Type V, typically from $\approx 12\%$ o-mode to $\approx 7\%$ x-mode. Many Type III/V bursts are isolated and are not associated with any reported flare or X-ray burst. However, when Type III's occur at the start of a flare, they tend to be intense, to be in groups of 10 or more, and to be followed by Type V continuum. Type V radiation occasionally blends into the flare continuum. While the emission process is not fully understood, Type V bursts are probably due to plasma radiation at the second harmonic, produced by the same electron stream that causes the Type III's; the longer duration of the Type V bursts is attributed to the presence in the stream of electrons that are slower than those normally present, and the change of sense of polarization is attributed to a change in the angular distribution of the Langmuir waves, from a highly collimated distribution in the Type III burst to a more widespread distribution during the Type V burst.

Decimetric Wavelength Bursts

The decimetric range, strictly from 300 MHz to 3 GHz but in terms of phenomenology from about 200 MHz to 1 or 2 GHz, displays perhaps the most complex and bewildering variety of bursts. In many cases the origin of

the bursts remains a mystery. Here we briefly describe two common varieties (Type III–like bursts and Type IV's) and mention a few kinds of fine structures that are sometimes present along with Type IV. Catalogs and descriptions of fine structures have been published by Bernold (1980) and Slottje (1981), and a review of theory has been presented by Kuijpers (1980).

Type III–like bursts in the decimetric range show many of the characteristics of their metric counterparts—fast drift rates, association with impulsive phases of flares—but are different in several respects (see, for example, Elgaroy 1980). Usually they are confined to a frequency range of 100 MHz or so and do not continue downward through the metric and decametric ranges. This implies that the electron streams presumably generating these bursts travel only short distances and do not continue moving outward along open field lines. Their drift rates are very large (typically 300 MHz s^{-1}), sometimes in the opposite sense than usual, and sometimes are immeasurably fast. They have very short durations of $\lesssim 0.3$ s. Their polarization does not seem to have been measured in a systematic way.

The interpretation of Type III–like bursts is uncertain. They likely originate in small-scale loops within a given active region. The drift rates, if interpreted as for normal Type III bursts, require both upward- and downward-moving electron streams and sometimes relativistic electrons. While the bursts probably originate from plasma radiation, the details of the emission mechanism may differ from that of normal Type III bursts, and a different excitation mechanism may be involved.

Decimetric Type IV bursts are characterized by continuum radiation extending over part of the range from ≈ 200 MHz to ≈ 1 GHz (see Figure 11). The radiation is distinguishable from its metric counterpart in being irregular and bursty, and from its microwave counterpart in having the opposite sense of circular polarization, i.e. it is in the sense of the o-mode. A wide variety of fine structures can be superimposed on the decimetric continuum (e.g. Slottje 1981): (*a*) pulsations with periods of $\gtrsim 1$ s, quasi-periodic and sometimes simultaneous over a 2:1 band of frequencies; (*b*) absorption features occurring over part or most of the band; (*c*) patterns of parallel, drifting emission bands ("zebra patterns"); (*d*) very narrow band bursts with low drift rates ("fiber bursts"); (*e*) bursts confined in frequency and time, with emission at the higher frequencies blending into absorption at the lower ("tadpole bursts"); and (*f*) spiky structures of duration ranging from <50 to ≈ 200 ms, bandwidth from <0.5 to (rarely) ≈ 10 MHz (average ≈ 2 MHz), and (in most but not all cases) high circular polarization ("spike bursts").

The interpretation of these decimetric bursts is complicated and

uncertain. The Type IV continuum is probably due to a form of plasma radiation, with the moderate ($\approx 50\%$) circular polarization implying radiation near the fundamental (e.g. Benz 1980). Kuijpers (1980) suggests that a high level of upper hybrid waves ($\omega_{UH}^2 = \omega_p^2 + \Omega_e^2$, where $\omega_p \gtrsim \Omega_e$ here) arises because a loss-cone anisotropy develops when electrons are trapped in magnetic loops. Some of this energy is then converted to electromagnetic waves by one of the processes described earlier. The fine structures presumably arise because the plasma and gyro frequencies are of the same magnitude in at least some parts of the source region, and many wave modes are therefore possible. The locations where ω_{UH} is an integer multiple $n\Omega_e$ of the cyclotron frequency seem to be particularly important; in these "double resonance" regions, instabilities tend to grow most rapidly. The decimetric "spike bursts" may be an extension to lower frequencies of the "microwave spike bursts" described below and are possibly due to the cyclotron maser.

Microwave Bursts

At the shorter wavelengths ($\lesssim 10$ cm, $f \gtrsim 3$ GHz), bursts generally arise from the low corona in the closed magnetic fields of active regions. There is a very close association between microwave and hard X-ray bursts, with the higher radio frequencies generally corresponding most closely to the harder X rays. Not only is the microwave flux density approximately proportional to the hard X-ray flux, but the temporal variations are often nearly identical, even to a time scale of < 1 s. Recent reviews of the properties of microwave bursts have been given by Marsh & Hurford (1982), Kundu & Vlahos (1982), and Kundu (1983).

Microwave impulsive bursts occur during the impulsive phase of flares (Figure 11), when the rate of energy release is highest, and their profiles are remarkably similar to those of impulsive hard X-ray bursts. VLA observations show that microwave impulsive bursts almost always originate in a set of magnetic loops that arch over the neutral line of the photospheric field. This result is found by direct comparison of radio maps with magnetograms, by the polarization of the radio waves (LH on one side of the source, RH on the other), and by the location of radio sources between Hα kernels that mark the footpoints of the set of loops into which fast electrons are precipitating. The radio source sizes usually increase with decreasing frequency, from $\approx 3''$ at 15 GHz to $\approx 30''$ at 1.4 GHz, presumably because the lower-frequency radiation comes from the larger, outer loops of a nested arcade. In contrast, for many flares the hard X-ray sources are at low altitudes, at the footpoints of the set of loops in which the radio sources exist. From this it is inferred that the hard X rays are due mainly to bremsstrahlung when fast electrons precipitate into regions of high density,

while the radio waves are due mainly to electrons (of the same accelerated population) that are trapped in the loops.

The evidence is strong that the radiation mechanism for the radio waves is gyrosynchrotron emission (predominantly x-mode) from electrons of energy ≈ 0.1 to 1 MeV, spiraling in a magnetic field of $B \approx 100$ to 500 G, and emitting at harmonics ≈ 10 to ≈ 50 of the gyrofrequency. The sources are usually optically thick at frequencies $\lesssim 10$ GHz and are optically thin at higher frequencies, which leads to spectra such as those sketched in Figure 2. It is not so clear what the energy distribution of the fast electrons is; possibilities include a near-Maxwellian of $T_e \approx 10^8$ to 10^9 K, a power law of energy spectral index $\delta \approx 3$ to 7, or a multicomponent distribution with different volumes at different effective temperatures. The last of these is implied by the observed increase of source size with decreasing frequency, a common trait of impulsive bursts and one which accounts for the fact that the radio spectral slope in the 1–10 GHz range is $\approx +1$, not $\geq \pm 2$ as would be true for a homogeneous source.

Microwave Type IV bursts are quite rare and occur only in association with large flares and shock waves. This radiation typically builds up over a period of a few minutes following the start of some flares as a portion of the first-phase electrons are further accelerated to relativistic energies, probably by Fermi acceleration involving a shock wave or shock-produced turbulence. The fast electrons are then left in coronal loops to radiate by the gyrosynchrotron process. The radiation intensity usually peaks near 3 to 10 cm, but it has a fairly broad range. Microwave Type IV's are closely associated with high-energy proton events observed on Earth.

Microwave postbursts occur fairly frequently in association with moderate to large flares. They are mainly visible in the late phase of flares as an enduring enhancement of flux after the stronger impulsive components have faded. It is believed that they result from thermal bremsstrahlung from the hot, dense plasma that remains in the low corona for some tens of minutes following flares, the same plasma that is the source of enhanced soft X-ray emission.

Microwave spike bursts, fairly recently identified (Dröge 1977, Slottje 1978, 1980, Zhao & Jin 1982), are characterized (as seen in Figure 12) by their short durations (milliseconds) and high degrees of circular polarization ($\approx 100\%$). The source sizes are inferred from the occasional ~ 1-ms rise times to be < 300 km, and the brightness temperatures to be $> 10^{13}$ K. The bursts have been observed in the range from a few hundred megahertz to possibly 5 GHz. Their bandwidths are very narrow, sometimes only a few megahertz. These characteristics, particularly the high brightness temperatures together with high circular polarizations, imply that these bursts result from a coherent radiation mechanism. The cyclotron maser (or one of

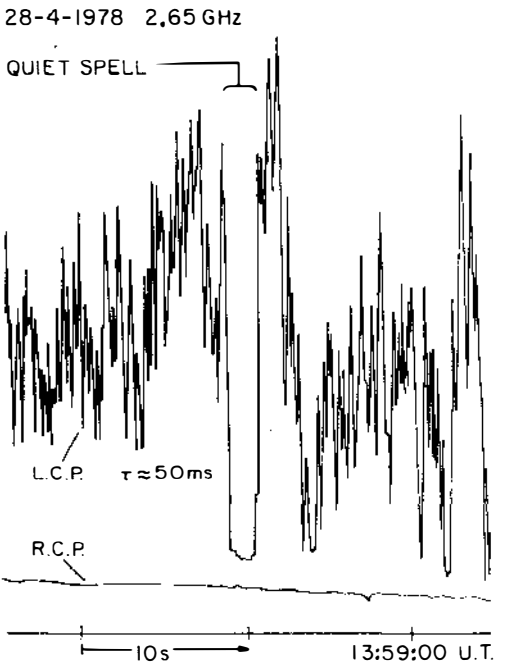

Figure 12 Microwave spike bursts from the Sun at 2.65 GHz, recorded with a time constant of 10 ms. In this event only LH-polarized spikes were recorded, some with variations on a 50-ms time scale. (From Slottje 1980.)

the related processes described above) is the most plausible mechanism. Similar bursts are observed at decametric to kilometric wavelengths coming from Earth ("auroral kilometric radiation"), from Jupiter and Saturn (decametric radiation), and from other stars (see below), and these are convincingly attributed to the cyclotron maser.

4. RADIO EMISSION FROM STARS

The numbers and kinds of stars detected at radio wavelengths have increased rapidly in the last few years, and new results are being published in nearly every issue of the major journals. In this section it is possible only to review the main characteristics of the emission from several kinds of stars. An attempt is made to identify the various radiation mechanisms, but it is not feasible to describe how the radio observations relate to the physics of the different kinds of stars. In several reviews more detailed remarks are given about various stellar radio phenomena and their relation with other

observations, e.g. Hjellming (1974), Feldman & Kwok (1979), Hjellming & Gibson (1980), and Gibson (1983).

Stellar Chromospheres, Coronae, and Activity

Over the past few years many astronomers were surprised to find that coronae exist on a wide variety of stars, quite unexpectedly for stars in certain parts of the HR diagram. Most evidence came from UV and X-ray observations, especially by IUE and the Einstein observatory. Meanwhile, solar studies have demonstrated that X rays from the quiet corona arise almost entirely in magnetic loops, and that a necessary and perhaps sufficient condition for coronae is the existence of magnetic fields.

To date, quiescent emission from several late-type stars has been detected at radio wavelengths (Gary & Linsky 1981, Topka & Marsh 1982, Linsky & Gary 1983). The example in Figure 13 shows that both dMe stars of the system EQ Peg are emitting (Topka & Marsh 1982). Measurements of radio flux density are not always consistent with models derived from the X-ray data. For example, for the star UV Ceti the radio data require the presence

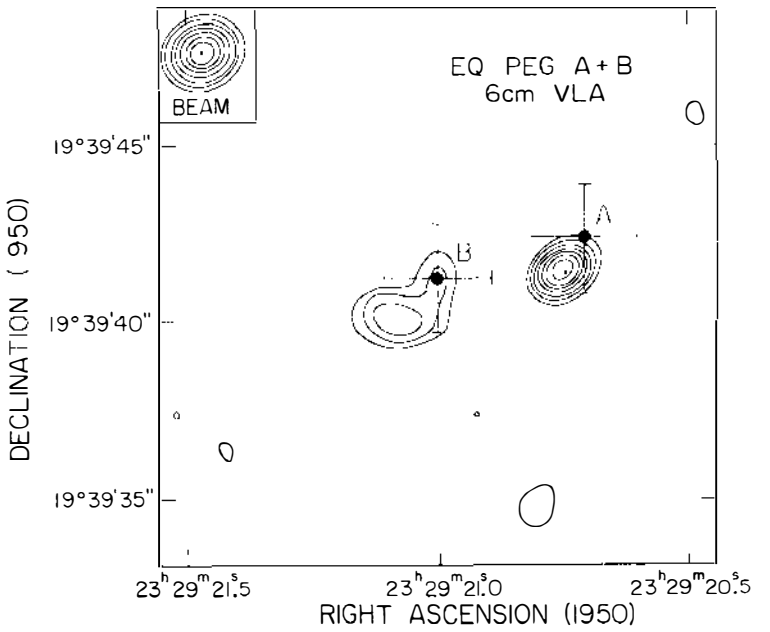

Figure 13 Quasi-steady radiation at 4.9 GHz recorded at the VLA from the two dMe stars of the well-separated binary EQ Peg. Stars A and B have flux densities of 0.6 and 0.4 mJy, respectively. The estimated optical positions of the two stars, with error bars, are shown. (From Topka & Marsh 1982.)

of higher-temperature material (several $\times 10^7$ K) or a more extended corona (several stellar radii) than one would have expected from X-ray data alone. Alternatively, a nonthermal tail of electrons with $E > 10$ keV could produce the observed radiation.

As is the case with the Sun, the emission from stellar coronae undoubtedly varies on several time scales, from day to day as active regions and starspots are born and die or rotate into and out of view, and from year to year in an activity cycle.

Flare Stars

Flares are common on certain kinds of stars, especially M dwarfs, and are seen at wavelengths from X ray to metric radio. The energies of the flares sometimes exceed those of their solar counterparts by several orders of magnitude. Several different emission mechanisms may be important at radio wavelengths—plasma, gyrosynchrotron, and cyclotron maser—and they can usually be distinguished by their spectra, polarization, and time variations. Figure 14 shows the time variability of one such stellar flare recorded at the VLA; interestingly, the quiescent emission arose from one star of a widely separated pair of dMe stars, and the burst arose from the other (Gary et al. 1982). The properties of the quiescent emission are compatible with the gyrosynchrotron mechanism, while those of the intense, highly circularly polarized burst are very similar to solar microwave spike bursts and imply a cyclotron maser. Another example is shown in Figure 15, recorded at Arecibo by Lang et al. (1983). This shows both a moderately polarized outburst lasting some tens of minutes, with time variations on a second to minute scale, and a strongly polarized component with variations on all scales down to the 200-ms resolution of the receiver. Again the properties suggest gyrosynchrotron emission for the longer-lived component and cyclotron maser emission for the rapidly varying, highly polarized component.

At meter wavelengths (here meaning $\nu \lesssim 500$ MHz) many thousands of hours have been spent observing flare stars, and many flares have been detected. The most powerful and long-lasting flares are the most noteworthy, both because they are most readily distinguishable from interference and because they place the greatest demands on theory. Measured flux densities imply radio luminosities much larger than those of solar flares at the same wavelengths, 10^4 times or more (e.g. Lovell 1969, Spangler & Moffett 1976, Davis et al. 1978). Brightness temperatures, derived from the measured fluxes and the assumption of source sizes smaller than the stellar disks, range from $\sim 10^{12}$ to $\gtrsim 10^{15}$ K. These values are of the same order to 100 times larger than those for solar Type IV bursts. In a few cases the polarization of the bursts has been recorded (e.g. Spangler et al. 1974). In

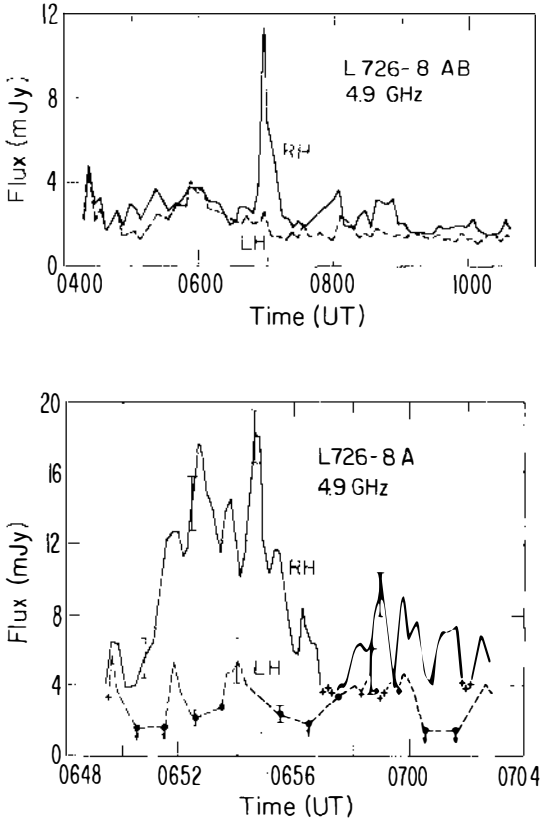

Figure 14 Radio emission at 4.9 GHz recorded at the VLA from the dMe stars UV Ceti and its companion L726-8A. The quasi-steady, nearly unpolarized emission of 2 mJy in the top panel is from UV Ceti, while the purely RH-polarized outburst is from L726-8A. In the bottom panel the flux during the outburst is plotted with 10-s resolution. (From Gary et al. 1982.)

one of the best-observed bursts the degree of circular polarization ranged from 50% to 80%, and that of linear polarization to 20%. The high brightness temperatures and moderate-to-high circular polarizations of these bursts strongly imply that the radiation process is coherent, but it is not immediately clear whether it is plasma radiation, cyclotron maser emission, or sometimes one or the other. If plasma radiation, the high degree of circular polarization implies it is at the fundamental. The linear polarization is very difficult to understand. Even though both plasma radiation and cyclotron maser emission can have an intrinsic linear component, one would expect from theory that linear polarization in the Sun and stars would be destroyed or made unobservable by Faraday

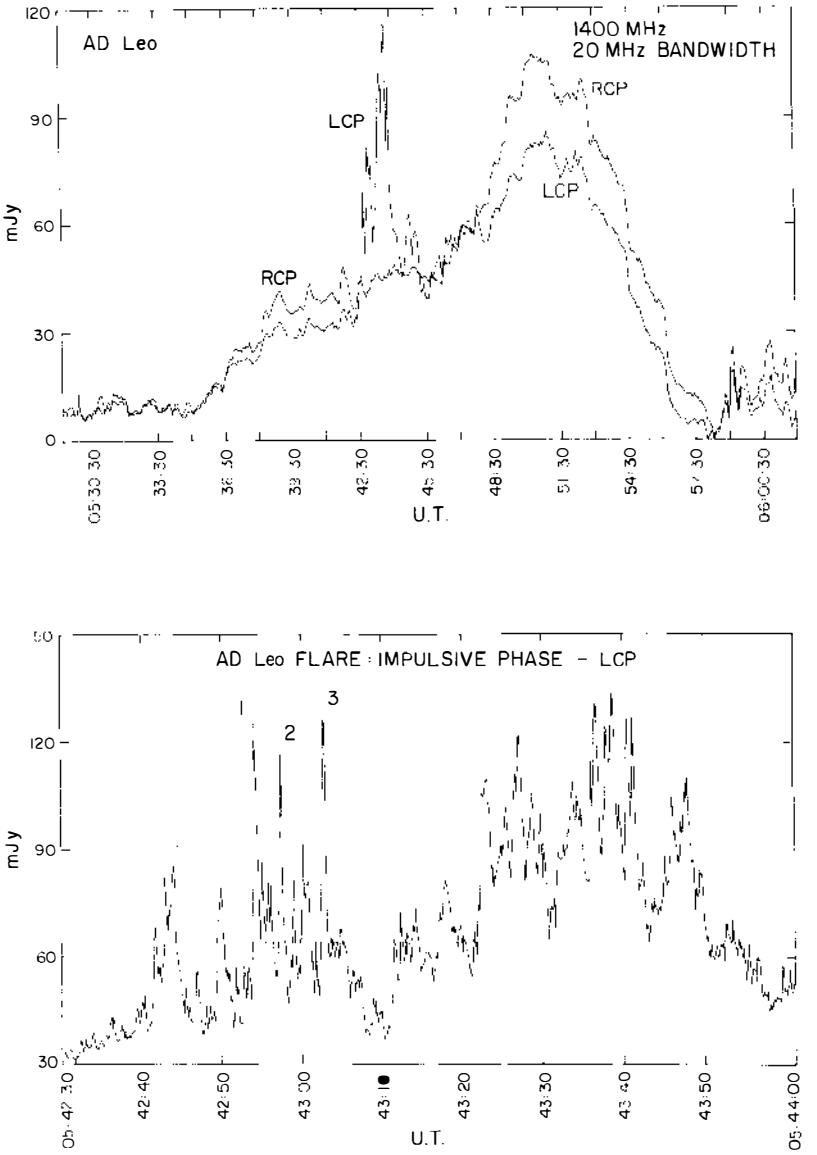

Figure 15 A radio burst at 1.4 GHz, recorded at Arecibo from the dMe star AD Leo. The top panel shows the overall burst, lasting about 30 min and having low-to-moderate circular polarization of about 15%. The bottom panel shows the purely LH-polarized portion. Even with a time resolution of 200 ms, the rise times of some spikes are not resolved. (From Lang et al. 1983.)

rotation in the overlying plasma. Observationally, for solar bursts, evidence for linear polarization has been reported and then contradicted; instrumental polarization (e.g. due to ground reflections or dish structures) is the likely explanation for the reports. However, if real, linear polarization is a very important diagnostic tool, and attempts to observe it with well-calibrated instruments should be continued.

Flare Stars and Stellar Evolution

An important discovery, made by G. Haro and W. Morgan in 1953, is that flares are common in T Tauri stars and stellar associations, implying that flare processes are stronger in the younger stars and that flaring may be important in the process of stellar formation and development. It may even be true that in the early stages of their lives, all stars pass through a stage of flare activity (e.g. Gurzadyan 1980). For example, of 175 T Tauri stars in the Orion association with hydrogen emission lines, 28 have flarelike activity at visible wavelengths on time scales of <30 min. Altogether 325 stars in Orion are known to flare, with spectral classes K0 to M3. Similarly, in the Pleiades, 469 stars of spectral class K2 to M5 have been known to flare at visible wavelengths.

It would be surprising if radio emission did not accompany the optical activity in many of these stars and associations. Many undoubtedly have magnetic fields and fast electrons. A search for radio emission at 150 and 408 MHz from the Orion association was made by Slee & Higgins (1971) and Tovmassian et al. (1974), and they obtained several detections of surprisingly powerful bursts, one with an implied brightness temperature of 10^{20} K. However, V. R. Venugopal (see Gibson 1983) observed for several hundred hours at 327 MHz and detected no similar bursts. Searches at centimeter wavelengths with the VLA are just beginning, and they will have the capability of measuring polarization and pinpointing which star is emitting. Because the distance to most of the stellar associations is some 30 times farther than to typical flare stars, the flux density is down by a factor of 1000 and is thus detectable only for the more intense flares, i.e. 10 to 1000 times more intense than the usual ones and more like those reported by Lovell (1969) from YZ CMi, Slee & Higgins (1971) from Orion, and by Dulk et al. (1983) from AM Herculis.

Because radio emission generally depends on the characteristics of the magnetic field, its detection from young stars should be expected and important: expected because magnetic fields and hence nonthermal radio bursts are likely to exist near newly formed stars, and important because magnetic fields probably play a crucial role in the initial stellar evolution (e.g. the spinning down of a protostar), and radio methods are perhaps the only way of detecting the fields and deriving their properties.

Stellar Winds

As with coronae, stellar winds are now known to exist in a wide class of stars: early types, late-type giants, and pre- or early main sequence (e.g. Bieging et al. 1982, Drake & Linsky 1983). In fact, most stars may have either a strong wind or a hot corona. In recent years, radio flux measurements have been used for accurate derivation of mass-loss rates; such measurements are free from some of the uncertainties that plague UV, optical, and IR observations. The resulting picture of mass losses is interesting in itself because of the new insight into hydrodynamics coupled with radiation; also, mass losses can influence the course of stellar evolution. Some aspects of interstellar physics and star formation are affected because interstellar mass gains and shock waves are associated with the stellar mass losses. Temporal changes in mass-loss rates from stars may also be important and should be prominent in radio flux measurements.

Generally, the radio radiation from stellar wind sources is believed to be due to bremsstrahlung from very large sources (hundreds of astronomical units, and larger at the lower frequencies) of plasma of $T \sim 10^4$ K. However, intense and variable radio flux has recently been detected from several O-type stars (White & Becker 1983, Abbott et al. 1984). The origin of this high-temperature or nonthermal radiation is not known; possibilities include the presence of gas with $T \gtrsim 3 \times 10^5$ K and accretion onto a relatively low mass ($< 10\ M_\odot$), distant ($> 50\ R_*$) companion.

Close Binary Stars

RS CVn–type binaries are probably the most common kind of radio-detected stars, with the possible exception of flare stars. Their radio emission is intense, highly variable, and often circularly polarized. About 30 have been detected (e.g. Mutel & Lestrade 1985). The RS CVn's are moderately close binary systems with periods of about 1 to 30 days, usually with one star being of spectral class G or later. Some have variable visible and UV emission, and dark areas (probably starspots) covering much of one star. Together with the properties of the X-ray emission, these characteristics imply that the systems involve mass transfer from one star to another and, perhaps most importantly, that they have intense magnetic fields, chromospheres, and coronae. It is believed that the strong magnetic fields are induced by tidally enforced rapid rotation. For many systems the fields of the two stars probably interact in the intervening medium, as depicted in Figure 16 (from Uchida & Sakurai 1983).

For RS CVn's there are at least two kinds of radio emission time scales and probably two radiation processes. First is the common component (e.g. Spangler et al. 1977, Feldman et al. 1978) that varies on time scales of hours

(individual flare events) and days (series of flare events) to months and possibly years. For some systems there may be a quiescent level, but this is not certain because of the frequent variations. Typically the radiation is moderately circularly polarized ($\lesssim 30\%$). In a few instances the radiation has been observed with VLB techniques (e.g. Lestrade et al. 1984). The sources typically are found to be resolved at 0.5 to 2.0 milliarcsec, which implies source sizes comparable with the binary separation or with an individual stellar diameter. For one flare event on UX Ari, VLB observations by Mutel et al. (1985) revealed the core-halo structure shown in Figure 17. These authors suggest that the core is due to an outburst in progress on the K0 IV star, and that the halo is due to fast electrons remaining trapped in the fields between the stars subsequent to one or more flares.

The brightness temperatures corresponding to typical flux densities and to the sizes measured by VLB range from $\sim 10^8$ to a few $\times 10^{10}$ K. In

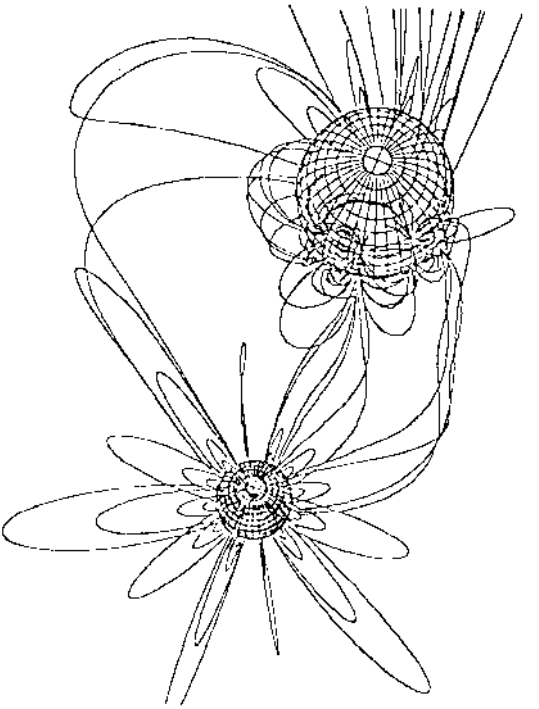

Figure 16 Diagram showing a hypothetical RS CVn system with interconnecting magnetic fields. Both stars were assumed to have scaled versions of the magnetic fields of solar active regions, and the overall magnetic field with interconnections was calculated from potential theory. (From Uchida & Sakurai 1983.)

combination with the moderate circular polarization observed (in general, lower polarization with higher brightness), the data are consistent with the mechanism of gyrosynchrotron radiation by electrons of a few MeV or less spiraling in fields of ~ 10 to ~ 100 G (e.g. Kuijpers & van der Hulst 1985).

The second kind of radiation from RS CVn binaries has a shorter time scale (minutes to hours) and a high circular polarization ($\approx 100\%$). Figure 18 shows simultaneous observations of HR 1099 at two frequencies made by Brown & Crane (1978). At the higher frequency of 8.1 GHz the flux and polarization are consistent with a gyrosynchrotron source as just described, while at the lower frequency of 2.7 GHz the large enhancement is seen only in one polarization. If we assume a source size less than a stellar diameter (no VLBI observations have yet been made of this kind of burst), the derived brightness temperature for that component is $>10^{11}$ K. Such high brightness and polarization require a coherent emission process such as the cyclotron maser.

Novae and dwarf novae represent another class of binary stars that have been detected at radio frequencies. The flux from novae is probably due to free-free emission from an expanding shell of hot, ionized gas (e.g. Hjellming 1974). Dwarf novae consist of a white dwarf that is accreting matter from a red dwarf companion in close proximity (binary periods $\lesssim 12$ hr). A

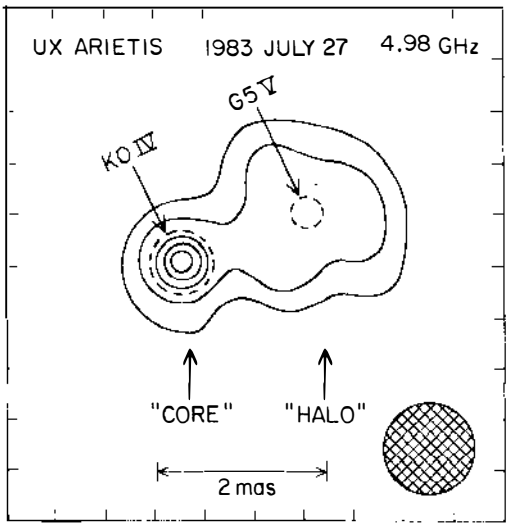

Figure 17 A very long baseline (VLB) map of the RS CVn system UX Ari during a period of relatively constant flux density. Both a core and a halo source are visible. The effective beamwidth of 1 milliarcsec is shown in the lower right corner. The relative positions and sizes of the two stars at the time of the observations are shown by the dashed circles, but their actual positions relative to the radio features are completely conjectural. (From Mutel et al. 1985.)

marginal ($<5\sigma$) detection of radio emission from a dwarf nova outburst was reported by Benz et al. (1983). The emission mechanism, whether gyrosynchrotron or cyclotron maser, cannot be determined from the sparse data available.

AM Herculis–type binaries are a class of magnetic cataclysmic variable stars, and radio emission has been detected from the prototype of the class, AM Her (Chanmugam & Dulk 1982, Dulk et al. 1983). The primary star of the system is a white dwarf with a surface field of about 10^7 G, sufficiently strong that the secondary (a red dwarf about 10^{11} cm distant) is embedded in the white dwarf's magnetosphere. Electromagnetic coupling and/or tidal effects from the small separations of these binaries enforce synchronous rotation at the binary periods of 1–3 hr. Two components of radio emission have been observed: quiescent and outburst. The suggested model for the quiescent component has $\sim$300-keV electrons trapped in either the magnetosphere of the white dwarf or the region of fields connecting the two stars, with the electrons emitting gyrosynchrotron radiation at harmonics ≈ 20 to ≈ 50 of the cyclotron frequency. Suggested ways of energizing the electrons include (*a*) magnetic interactions of the fields of the two stars and (*b*) operation of a unipolar inductor, with the red dwarf in the white dwarf's magnetosphere being analogous to Io in Jupiter's magnetosphere. The quiescent emission is visible in Figure 19 (*top panel*).

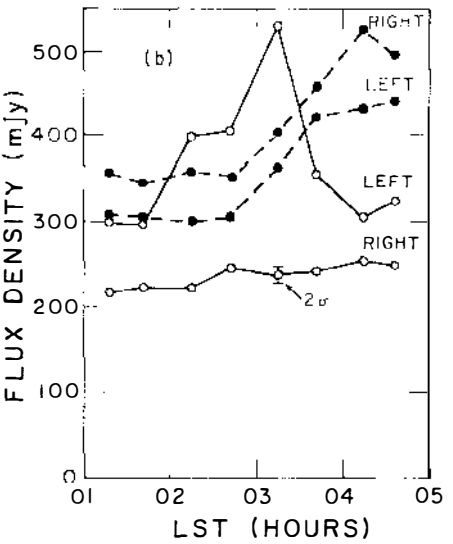

Figure 18 Flux density of the RS CVn system HR 1099 as recorded in LH and RH circular polarization at 2.7 GHz (solid curves) and 8.1 GHz (dashed curves). A typical 2σ error bar is shown. Note that the major flux increase occurred only in LH polarization at 2.7 GHz. (From Brown & Crane 1978.)

On the occasion of the observations shown in Figure 19 (*middle and bottom panels*), an outburst of radio emission was detected that had rapid time variability ($\lesssim$10 s), high brightness ($>10^{11}$ K), and high circular polarization ($\approx$100%). These characteristics again imply a coherent

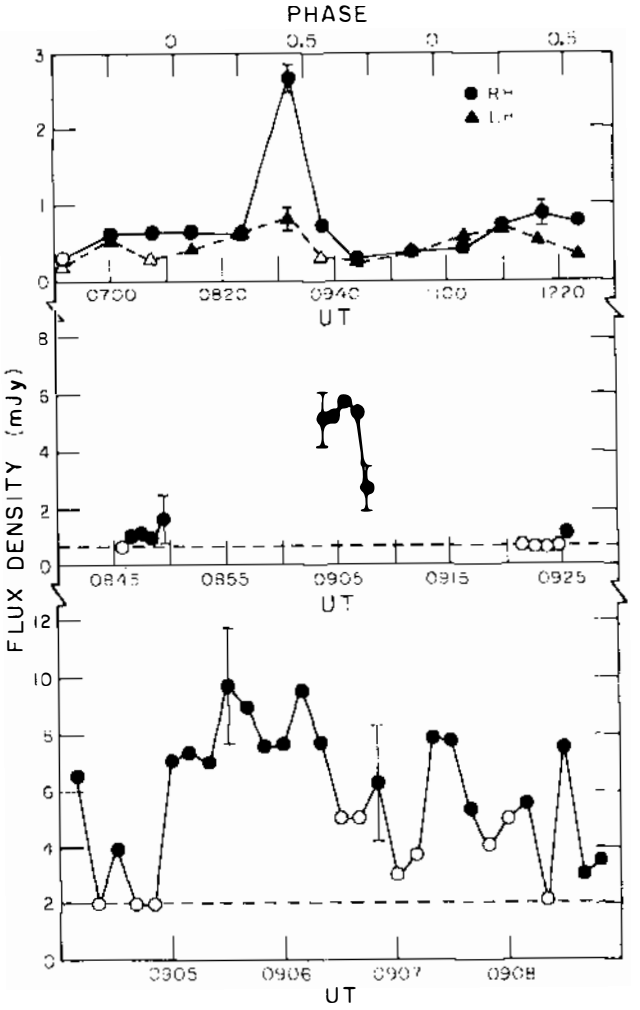

Figure 19 Time-intensity plots of the 4.9-GHz emission from AM Herculis recorded at the VLA. The top panel shows $\approx$30-m averages of the data over about 6 hr; an outburst is seen in one data point in RH polarization. The middle panel shows 5-m averages of the three scans encompassing the outburst; in the intervals of missing data, the VLA was operating at 2 cm and no emission was recorded. The bottom panel shows the central 5-min scan at the finest time resolution then available at the VLA (10 s). Typical $\pm 1\sigma$ error bars are shown. (From Dulk et al. 1983.)

radiation mechanism, probably the cyclotron maser. The spectrum of the outburst is unknown; it was detected at 5 GHz (implying a field strength in the source region of ≈ 1000 G) but not at 15 GHz (for which ≈ 3000 G is needed). The probable location of the source was inferred to be on or near the red dwarf, which implies that the red dwarf has its own intrinsic field. Thus there is the likelihood of magnetic interactions between the fields of the two stars. The previously unexplained variations in X-ray, UV, and optical activity on time scales of months could result from such interactions modulating the transfer of matter from the red dwarf to the white dwarf.

5. CONCLUSIONS

In this review we have attempted to coordinate and simplify the main features of theory and observations of solar and stellar radio emissions. The Sun has revealed to us a large variety of radio emissions that can occur in differing circumstances, with the incoherent emission mechanisms being bremsstrahlung and gyrosynchrotron radiation, and the coherent mechanisms being cyclotron masers and plasma radiation. Observed or inferred brightness temperatures range up to 10^{15} K, which implies coherent radiation mechanisms for those bursts of brightness greater than 10^9 or 10^{10} K.

Spectacular discoveries have recently been made of quite unexpected radio emissions from stars; examples are the bright, highly polarized bursts from flare stars and close binaries, and the "nonthermal" nonbremsstrahlung radiation from unexpectedly hot or energetic electrons in stellar wind sources. Already some 30% of the time on the VLA is devoted to stellar observations, and one has the feeling that numerous other stellar radio phenomena have yet to be discovered or properly explored. Reasons for this conclusion include the following: (*a*) The sources have flux densities near or just below the present sensitivity limit of the VLA; (*b*) they are outside its frequency range; (*c*) they are not quite resolvable with the present VLA; and (*d*) they are too weak to be detected with present very long baseline (VLB) networks. But new and improved radio telescopes are now being constructed or planned (for example, VLB arrays, an Australian telescope, and an augmented VLA with increased sensitivity, frequency coverage, and resolution). With these improvements, many of the present problems will be solved, and undoubtedly new phenomena will be revealed.

ACKNOWLEDGMENTS

This review is dedicated to the memory of Dr. S. F. Smerd, whose exceptional insight into radio emission processes and solar radiophysics was an inspiration. I thank D. B. Melrose and D. E. Gary for stimulating

discussions and helpful comments. Part of this work was sponsored by NASA's Solar Heliospheric Physics and Solar Terrestrial Theory programs under grants NSG-7287 and NAGW-91 to the University of Colorado.

Literature Cited

Abbott, D. C., Bieging, J. H., Churchwell, E. 1984. *Ap. J.* 280:671

Benson, R. F. 1982. *Geophys. Res. Lett.* 9: 1120

Benson, R. F. 1984. *Radio Sci.* 19:243

Benz, A. O. 1980. *Ap. J.* 240:892

Benz, A. O., Furst, E., Kiplinger, A. L. 1983. *Nature* 302:45

Bernold, T. 1980. *Astron. Astrophys. Suppl.* 42:43

Bieging, J. H., Abbott, D. C., Churchwell, E. 1982. *Ap. J.* 263:207

Bougeret, J. L. 1985. In *Collisionless Shock Waves in the Heliosphere, Am. Geophys. Union Monogr.*, ed. R. G. Stone, B. T. Tsurutani. In press

Brown, R. L., Crane, P. C. 1978. *Astron. J.* 83:1504

Chanmugam, G., Dulk, G. A. 1982. *Ap. J. Lett.* 255:L107

Davis, R. J., Lovell, B., Palmer, H. P., Spencer, R. E. 1978. *Nature* 273:644

Drake, S. A., Linsky, J. L. 1983. *Ap. J. Lett.* 274:L77

Dröge, F. 1977. *Astron. Astrophys.* 57:285

Dulk, G. A., Bastian, T. S., Chanmugam, G. 1983. *Ap. J.* 273:249

Dulk, G. A., Gary, D. E. 1983. *Astron. Astrophys.* 124:103

Dulk, G. A., Marsh, K. A. 1982. *Ap. J.* 259:350

Dulk, G. A., McLean, D. J. 1978. *Sol. Phys.* 57:279

Dulk, G. A., Melrose, D. B., White, S. M. 1979. *Ap. J.* 234:1137

Elgaroy, O. 1980. *Astron. Astrophys.* 82:308

Feldman, P. A., Kwok, S. 1979. *J. R. Astron. Soc. Can.* 73:271

Feldman, P. A., Taylor, A. R., Gregory, P. C., Seaquist, E. R., Balonek, T. J., Cohen, N. L. 1978. *Astron. J.* 83:1471

Gary, D. E., Linsky, J. L. 1981. *Ap. J.* 250:284

Gary, D. E., Linsky, J. L., Dulk, G. A. 1982. *Ap. J. Lett.* 263:L79

Gibson, D. M. 1983. In *Activity in Red Dwarf Stars, IAU Colloq. No. 71*, ed. M. Rodono, P. Byrne, p. 273. Dordrecht: Reidel

Ginzburg, V. L., Syrovatskii, S. I. 1969. *Ann. Rev. Astron. Astrophys.* 7:375

Ginzburg, V. L., Zheleznyakov, V. V. 1958. *Astron. Zh.* 35:694 (Engl. transl. in *Sov. Astron.-AJ* 2:653)

Goldman, M. V. 1983. *Sol. Phys.* 89:403

Grognard, R. J.-M. 1985. See McLean & Labrum 1985, Chap. 11

Gurzadyan, G. A. 1980. *Flare Stars.* Oxford: Pergamon. 344 pp.

Hewitt, R. G., Melrose, D. B., Dulk, G. A. 1983. *J. Geophys. Res.* 88:10065

Hewitt, R. G., Melrose, D. B. 1985. *Sol. Phys.* In press

Hewitt, R. G., Melrose, D. B., Rönnmark, K. G. 1981. *Proc. Astron. Soc. Aust.* 4:221

Hewitt, R. G., Melrose, D. B., Rönnmark, K. G. 1982. *Aust. J. Phys.* 35:447

Hjellming, R. M. 1974. In *Galactic and Extragalactic Radio Astronomy*, ed. G. L. Verschuur, K. I. Kellermann, p. 159. New York: Springer-Verlag

Hjellming, R. M., Gibson, D. M. 1980. See Kundu & Gergely 1980, p. 209

Holman, G. D., Eichler, D., Kundu, M. R. 1980. See Kundu & Gergely 1980, p. 457

Kai, K., Melrose, D. B., Suzuki, S. 1985. See McLean & Labrum 1985, Chap. 16

Krüger, A. 1979. *Introduction to Solar Radio Astronomy and Radio Physics.* Dordrecht: Reidel. 330 pp.

Kuijpers, J. 1980. See Kundu & Gergely 1980, p. 341

Kuijpers, J., van der Hulst, J. M. 1985. *Astron. Astrophys.* In press

Kundu, M. R. 1965. *Solar Radio Astronomy.* New York: Interscience. 660 pp.

Kundu, M. R. 1983. *Sol. Phys.* 86:205

Kundu, M. R., Gergely, T. E., eds. 1980. *Radio Physics of the Sun, IAU Symp. No. 86.* Dordrecht: Reidel. 475 pp.

Kundu, M. R., Vlahos, L. 1982. *Space Sci. Rev.* 32:405

Lang, K. R. 1980. *Astrophysical Formulae.* New York: Springer-Verlag. 783 pp.

Lang, K. R., Bookbinder, J., Golub, L., Davis, M. 1983. *Ap. J. Lett.* 272:L15

Lee, L. C., Kan, J. R., Wu, C. S. 1980. *Planet. Space Sci.* 28:703

Lestrade, J. F., Mutel, R. L., Phillips, R. B., Webber, J. C., Niell, A. E., Preston, R. A. 1984. *Ap. J. Lett.* 282:L23

Lin, R. P., Potter, D. W., Gurnett, D. A., Scarf, F. L. 1981. *Ap. J.* 251:364

Linsky, J. L., Gary, D. E. 1983. *Ap. J.* 274:776

Lovell, B. 1969. *Nature* 222:1126

Marsh, K. A., Hurford, G. J. 1982. *Ann. Rev. Astron. Astrophys.* 20:497

McLean, D. J., Labrum, N. R., eds. 1985. *Solar Radiophysics.* Cambridge: Cambridge Univ. Press. 520 pp.

Melrose, D. B. 1971. *Astrophys. Space Sci.* 12:172

Melrose, D. B. 1980a. *Plasma Astrophysics*, Vol. 1. Dordrecht: Gordon & Breach. 269 pp.
Melrose, D. B. 1980b. *Plasma Astrophysics*, Vol. 2. Dordrecht: Gordon & Breach. 423 pp.
Melrose, D. B. 1980c. *Space Sci. Rev.* 26: 3
Melrose, D. B. 1981. *Proc. Astron. Soc. Aust.* 4: 139
Melrose, D. B. 1985a. See McLean & Labrum 1985, Chap. 8
Melrose, D. B. 1985b. See McLean & Labrum 1985, Chap. 9
Melrose, D. B., Dulk, G. A. 1982a. *Ap. J.* 259: 844
Melrose, D. B., Dulk, G. A. 1982b. *Ap. J. Lett.* 259: L41
Melrose, D. B., Dulk, G. A. 1984. *Ap. J.* 282: 308
Melrose, D. B., Dulk, G. A., Gary, D. E. 1980. *Proc. Astron. Soc. Aust.* 4: 50
Melrose, D. B., Hewitt, R. G., Dulk, G. A. 1984. *J. Geophys. Res.* 89: 897
Melrose, D. B., Nelson, G. J. 1985. See McLean & Labrum 1985, Chap. 13
Mutel, R. L., Lestrade, J. F. 1985. *Astron. J.* 90: 493
Mutel, R. L., Lestrade, J. F., Preston, R. A., Phillips, R. B. 1985. *Ap. J.* 289: 262
Omidi, N., Gurnett, D. A. 1982. *J. Geophys. Res.* 87: 2377
Petrosian, V. 1981. *Ap. J.* 251: 727
Robinson, P. A., Melrose, D. B. 1984. *Aust. J. Phys.* 37: 675
Robinson, R. D. 1985. See McLean & Labrum 1985, Chap. 15
Saito, K. 1970. *Ann. Tokyo Astron. Obs. Ser. 2* 12: 53
Scheuer, P. A. G. 1960. *MNRAS* 120: 231
Schneider, J. 1959. *Phys. Rev. Lett.* 2: 504
Sharma, R. R., Vlahos, L. 1984. *Ap. J.* 280: 405
Sharma, R. R., Vlahos, L., Papadoupoulos, K. 1982. *Astron. Astrophys.* 112: 377
Slee, O. B., Higgins, C. S. 1971. *Aust. J. Phys.* 24: 247
Slottje, C. 1978. *Nature* 275: 520
Slottje, C. 1980. See Kundu & Gergely 1980, p. 195
Slottje, C. 1981. *Atlas of Fine Structures of Dynamic Spectra of Solar Type IV and Some Type II Radio Bursts.* Utrecht: Neth. Found. Radio Astron. 200 pp.
Smith, D. F., Brown, J. C. 1980. *Ap. J.* 242: 799
Spangler, S. R., Moffett, T. J. 1976. *Ap. J.* 203: 497
Spangler, S. R., Owen, F. N., Hulse, R. A. 1977. *Ap. J.* 82: 989
Spangler, S. R., Rankin, J. M., Shawhan, S. D. 1974. *Ap. J. Lett.* 194: L43
Stewart, R. T. 1985. See McLean & Labrum 1985, Chap. 14
Suzuki, S., Dulk, G. A. 1985. See McLean & Labrum 1985, Chap. 12
Svestka, Z. 1976. *Solar Flares.* Dordrecht: Reidel. 399 pp.
Topka, K., Marsh, K. A. 1982. *Ap. J.* 254: 641
Tovmassian, H. M., Haro, G., Webber, J. C., Swenson, G. Jr., Yang, K. S., et al. 1974. *Astrofizika* 10: 337 (Engl. transl. *Astrophysics* 10: 212)
Twiss, R. Q. 1958. *Aust. J. Phys.* 11: 564
Uchida, Y., Sakurai, T. 1983. In *Activity in Red Dwarf Stars, IAU Colloq. 71*, ed. M. Rodono, P. Byrne, p. 629. Dordrecht: Reidel
Vlahos, L., Sharma, R. R. 1984. *Ap. J.* 280: 405
Vlahos, L., Sharma, R. R., Papadoupoulos, K. 1983. *Ap. J.* 275: 374
White, R. L., Becker, R. H. 1983. *Ap. J. Lett.* 272: L19
Wild, J. P., Smerd, S. F., Weiss, A. A. 1963. *Ann. Rev. Astron. Astrophys.* 1: 291
Winglee, R. M. 1985. *Ap. J.* In press
Wu, C. S., Lee, L. C. 1979. *Ap. J.* 230: 621
Zhao, R. Y., Jin, S. Z. 1982. *Sci. Sin Ser. A* 25(4): 422